Instabilities in conventional and unconventional ferrofluids

Dissertation
zur Erlangung des Grades
des Doktors der Naturwissenschaften
der Naturwissenschaftlich-Technischen Fakultät II
der Universität des Saarlandes
von

Andrey Ryskin

Mainz

2004

Tag des Kolloquiums: 04. 05. 2004

Dekan:	Prof. Dr. Th. Wichert
Gutachter:	Prof. Dr. H. Pleiner
	Prof. Dr. M. Lücke

Zusammenfassung

In dieser Arbeit werden hydrodynamische Instabilitäten in neuen künstlichen Materialien, Ferrofluide und Ferronematen, theoretisch untersucht. Ferrofluide sind kolloidale Suspensionen magnetischer Nanoteilchen in einer gewöhnlichen Füssigkeit, wie Wasser oder Benzol. Benutzt man einen nematischen Flüssigkristall als Trägerflüssigkeit, so erhält man Ferronematen. Ferrofluide sind in vielerlei Hinsicht sehr spezielle Flüssigkeiten. Sie sind superparamagnetisch, d.h. obwohl im Gleichgewicht die magnetischen Momente der Nanoteilchen ungeordnet sind, genügt schon ein schwaches Magnetfeld, um diese Momente auszurichten und eine große induzierte Sättigungsmagnetisierung zu erhalten. Diese Eigenschaft wird vor allem bei technischen und medizinischen Anwendungen benutzt. Ferner ist die Mobilität der Nanopartikel sehr gering verglichen mit der der Flüssigkeitsmoleküle, was zu einer extrem langsamen Diffusionsdynamik führt. Sehr groß sind dagegen die Dichteunterschiede zwischen Kolloid und Flüssigkeit. Diese beiden Eigenschaften, die sich in einer Beschreibung als binäre Mischung durch eine kleine Lewis-Zahl und einen grossen Thermodiffusions- oder Soretkoeffizienten bemerkbar machen, sind wesentlich für das spezielle Verhalten bei thermischen Konvektionsinstabilitäten, welches in Kapitel 2 (ohne) und in Kapitel 3 (mit Magnetfeld) diskutiert wird. Ferronematen zeichnen sich, verglichen mit gewöhnlichen Nematen, durch eine große Suszeptibilität gegenüber Magnetfeldern aus, was es erlaubt, auch üblicherweise vernachlässigte Magnetfeldeffekte in der Nematodynamik zu betrachten. Die Auswirkung solcher Effekte auf hydrodynamische Instabilitäten wird im 4. Kapitel behandelt.

Ferrofluide werden wegen der geringen Diffusivität der Magnetpartikel oft als Einkomponentenflüssigkeiten beschrieben. Wir zeigen in Kapitel 2, dass dies für die Beschreibung thermischer Konvektion nicht ausreicht. Beschreibt man das System als binäre Mischung mit der Konzentration der Nanoteilchen als zweiter Spezies, so machen sich die besonderen Eigenschaften der Ferrofluide bemerkbar. Insbesondere hat man nicht die Stabilität eines Zustands mit voll entwickeltem linearen Konzentrationsprofil zu betrachten, sondern es ist von einem sich gerade erst entwickelnden Profil auszugehen, das abgesehen von einer sehr dünnen Randschicht fast überall konstant ist. Für den hier betrachteten Fall, bei dem der angelegte Temperaturgradient und die Thermodiffusion in dieselbe Richtung zeigen, führt der große Soret-Koeffizient zu einer drastischen Verringerung der Instabilitätsschwelle. Dies ist aber nicht beobachtbar, da hier die Dynamik der sich entwickelnden Konvektionsstruktur extrem langsam ist. Betrachtet man das System in der Nähe der viel höheren Einkomponentenflüssigkeitsschwelle (welche man ohne Soret-Koeffizienten hätte) so ist das System dort instabil. Es ist dann sinnvoll, die linearen Anwachsraten der Instabilität (und nicht die Schwelle selbst) zu betrachten. In diesem Bereich sind die Zeitskalen wieder kurz genug und experimentell zugänglich. Als nächstes wird das nichtlineare Verhalten mittels eines normalen Galerkinverfahrens untersucht. Dabei zeigt sich, dass die Amplitude einer Störung des Grundzustands in Form von stationären Konvek-

tionsrollen sättigt. Dies ist im Widerspruch zu einer kürzlich aufgestellten Hypothese einer konvektiven Oszillation auf Grund der stark verschiedenen Zeitskalen von Wärmeleitung und Diffusion, stimmt aber mit Messungen von S. Odenbach überein, der unser Bild dieser speziellen binären Mischungs-Instabilität in Ferrofluiden bestätigt.

Im folgenden Kapitel wird die thermische Konvektion von Ferrofluiden im externen Magnetfeld beschrieben. Dafür wird zuerst das volle System der hydrodynamischen Gleichungen für magnetische binäre Mischungen ausgehend von fundamentalen thermodynamischen Prinzipien hergeleitet. Wir zeigen, dass die Beschreibung als binäre Mischung beschränkt ist, da für sehr hohe Magnetfelder das System thermodynamisch instabil wird. Möglicherweise hängt dies mit Teilchenagglomeration und Kettenbildung zusammen, wobei aber solche Aussagen eigentlich vom makroskopischen Standpunkt aus nicht zu machen sind. Für erlaubte Magnetfelder bestimmen wir die Sättigungsamplitude der thermischen Konvektion. Auf Grund der magnetischen Randbedingung spielt nun die Grenzschicht eine wichtige Rolle (im Gegensatz zum feldfreien Fall) und muss explizit betrachtet werden. Das Grenzschichtproblem wird analytisch behandelt unter zu Hilfenahme der numerischen Lösung. Die numerische Untersuchung der nichtlinearen Zeitentwicklung der konvektiven Strömung zeigt, dass wie im feldfreien Fall die Amplitude im Zustand eines stationären Rollenmusters sättigt. Mit Hilfe der analytischen Grenzschichtlösung lässt sich analytisch eine genäherte implizite Formel für die Sättigungsamplitude herleiten, die die Abhängigkeit von den Systemparametern angibt.

Im abschließenden Kapitel betrachten wir Instabilitäten in Ferronematen. Wie kürzlich gezeigt wurde, gibt es in Ferronematen Zusätze zu den hydrodynamischen Materialtensoren, die linear im externen Feld sind. Im Prinzip existieren solche Effekte auch in gewöhnlichen Nematen, aber in Ferronematen kann man erwarten, dass die phänomenologischen Transportkoeffizienten, die diese Effekte bestimmen, viel größer sind. Es ist ziemlich schwierig, diese neuen Effekte direkt zu messen, da sie sehr kompliziert sind. Deshalb ist es experimentell evtl. einfacher, solche Materialparameter indirekt mittels Instabilitäten zu bestimmen, wo sie für neue Aspekte des Instabilitätsverhaltens verantwortlich sind, insbesondere wenn es sich um qualitativ neuartige Phänomene handelt. Wir untersuchen theoretisch den Einfluss solcher neuer Terme auf die thermische Konvektions- (Rayleigh-Bénard) und die Fingerinstabilität (Saffman-Taylor) in Ferronematen im starken externen Magnetfeld. Wir finden, dass diese Instabilitäten ihren Charakter qualitativ verändern, da eine endliche Vortizitätsströmungskomponente parallel zum Feld auftritt – ein Phänomen, das in gewöhnlichen Flüssigkeiten bekannt ist für den Fall einer aufgeprägten Rotation (statt des Feldes). Die daraus resultierenden Zusatzeffekte (Strömung entlang der Konvektionsrollen, Schrägrollen, Rotation der Instabilitätsfinger) kann für die Messung der besagten phänomenologischen Transportparameter genutzt werden. Da diese Effekte linear im äußeren Feld sind und sich damit umkehren, wenn das Feld umgekehrt wird, sind sie deutlich von allen Feldeffekten zu unterscheiden, die auf intrinsischen Magnetfeldabhängigkeiten konventioneller Materialparameter beruhen, da letztere quadratisch im Feld und damit invariant bei Feldumkehr sind.
(translated by H. Pleiner)

Contents

Chapter 1

Introduction

1.1 Ferrofluids

Ferrofluids are suspensions of nano-sized ferromagnetic particles in some carrier liquid [1]. Without an applied external magnetic field the orientations of the magnetic moments of the particles are random resulting in a vanishing macroscopic magnetization (magnetic disorder). An external magnetic field, however, easily orients the particles' magnetic moments and a large (induced) magnetization is obtained. This "superparamagnetic" property is the basis for many applications [1].

The preparation of the magnetic particles is itself a complicated task. The main problem is that the ferroparticles should be more or less homogeneously distributed in the carrier liquid - the problem of stability. This problem appears due to the fact that particles attract each other due to van der Vaals and dipole moment interactions. For different purposes different kind of carrier liquids and magnetic particles are used. The carrier liquid can be water, oil, mercury etc. and one can also use different kind of particles - cobalt, magnetite etc. [1]. For each combination carrier-ferroparticles the problem of stability has to be solved independently. There are two most widely used ways of stabilization - steric stabilization and electrostatic stabilization. In electrostatic stabilization one uses charged particles to compensate the attractive forces by electrostatic repulsion. In steric stabilization repulsion forces due to a polymer coating of the particles are employed. When particles come close to each other the excluded volume repulsion becomes effective.

A major feature of ferrofluids is the bulk Kelvin force, which acts when a gradient of a magnetic field is present. This new force being incorporated into the equations of the fluid motion leads to many different effects, some of which have found technical applications. For example, viscous damping in loudspeakers, sealing and lubrication of hard disc axes etc. [1]. But probably most important are applications of ferrofluids in the medical domain. Applying the Kelvin force, for example, ferrofluids can be used to deliver certain drugs to a certain area of the body [2]. There is also the idea to use ferrofluids for cancer treatment by heating the tumor soaked in ferrofluids by means of an alternating external magnetic field [3].

In ferrofluids there are new kinds of instabilities. Rosensweig surface instability is a representative example [1]. But even the instabilities well-known from non-magnetic fluids, like Faraday [4–6], Rayleigh-Bénard [7–11], Couette-Taylor [12–14], and Safman-Taylor instabilities [15–17], show qualitatively new behavior, when considered for ferrofluids in the presence of

a magnetic field.

Apart from the Kelvin force, there are a lot of interesting physical effects involved with ferrofluids, for example, agglomeration and chain formation of magnetic grains [18] with drastic consequences like a complex rheological behavior [19–21], the different types of the relaxation of the magnetization - Neel and Brownian, that manifest themselves in the rotational viscosity [1], and thermodiffusion effects, which lead to binary mixture behavior [9–11].

There are many publications, which give a description of ferrofluids on the macroscopic, continuum level [1, 22]. To give a complete description, which reflects all the features of the macroscopic ferrofluid behavior, is probably a too complicated and unnecessary task, since many effects exist in principle, but can be neglected depending on the ferrofluid and external conditions present. But it is very important to find out what kind of description is appropriate for a certain ferrofluid under certain conditions. The investigation of instabilities in ferrofluids gives a good chance to test different approaches in the ferrofluid description and to determine what kind of effects are to be taken into account and which of them can safely be disregarded given the special ferrofluid and external conditions.

Ferrofluids have two constituents – carrier liquid and magnetic grains. In some cases diffusion of the magnetic grains can be important. It has been shown, for example, that the Soret or thermodiffusion effect is rather pronounced in ferrofluids [23]. A flux of particles [24] can also be created by a magnetic field gradient, the so called magnetophoretic effect. In these cases, when the flux of magnetic particles takes place, the appropriate way to describe ferrofluids is to use the model of a binary mixture.

Although ferrofluids are a very specific kind of binary mixture [9–11], there is a lot they have in common with the conventional well-studied binary mixtures, like an ethanol-water mixture, for example.

1.2 Binary mixtures

Thermal convection in binary mixtures like ethanol-water, ^3He-^4He, or various gas mixtures shows a rich spectrum of pattern formation behavior [25–27]. The spatiotemporal properties of convection in mixtures are more complex than those of one-component fluids due to the influence of Soret-sustained concentration gradients. The structural dynamics of the concentration distribution in mixtures results from an interplay between three competing mechanisms: nonlinear advection and mixing, weak solutal diffusion, and the Soret or thermodiffusion effect. The relative importance of the Soret effect is measured by the separation ratio ψ. When $\psi = 0$, we have a one-component liquid. In this case any concentration variations diffuse away. For non vanishing ψ, however, the external temperature gradient sustains the concentration variations against the advective and diffusive homogenization.

The concentration variation creates the buoyancy force. Depending on the sign of the separation ratio ψ, the solutal buoyancy force may act in the same direction as the usual temperature buoyancy force (the case, when $\psi > 0$), or counteract to this force (the case, when $\psi < 0$). Via the solutal buoyancy force, concentration field changes the momentum balance of the fluid and directly influence the flow, which in turn changes and mixes the concentration. This feedback causes different effects that cannot be observed in the one-component liquid convection.

For positive separation ratio ($\psi > 0$), the bifurcation from the conductive state is supercritical and stationary, as it is in the one-component liquid. But close to onset we have different kinds of patterns and secondary instabilities – square to roll instability, oscillatory instability, cross roll instability and others, depending on the combination of the binary mixture parameters [28–31].

When the separation ratio is negative ($\psi < 0$), the bifurcation picture and nonlinear structures are more complicated. In this case we have subcritical bifurcation and oscillatory bifurcation [25–27]. In nonlinear regimes we can have traveling waves, standing waves, and localized traveling waves (solitons) [27, 32–36].

1.3 Ferronematics

Nematic liquid crystals doped with single-domain ferro- or ferrimagnetic grains, usually denoted as ferronematics, are of great interest for potential applications, but also under the scope of fundamental research. Starting with the pioneering work of Brochard and de Gennes [37] the idea is to intensify the ponderomotive response of a nematic liquid crystal by doping it with a small amount of ferromagnetic particles. The strong orientational coupling between the magnetic grains and the surrounding nematogen matrix enhances the susceptibility of the director dynamics. Indeed, the magnetic field strength necessary to affect the director is decreased by several orders of magnitude giving control over the orientational state of the liquid crystal by magnetic fields as weak as 100 Oe. This "superparamagnetic" response is the basis of many applications. The original expectation that the nematic ordering induces magnetic order and thus leads to a spontaneous macroscopic magnetization (ferromagnetic state) has not been materialized until now.

Considerable efforts were undertaken in the preparation of various colloidal dispersions of ferromagnetic particles in liquid crystals during recent years. Starting with the first report in 1970 of mixing magnetic grains with the nematic phase of MBBA [38], there was a number of reports on the production of mixtures of rod-like and disk-like, thermotropic as well as lyotropic nematics with magnetic grains [38–41]. However, these systems were more like dirty liquid crystals, where the magnetic additives served for a better orientation of the nematics in an external field. Problems were the stability of these mixtures and the mutual orientation of the director and the magnetization. The experimental situation changed considerably, when it was possible to make stable emulsions, first as ferrosmectic systems [42–45], were the ferromagnetic nano-particles are embedded in the smectic layers. These ferrosmectics are very dilute systems, which prevents their use in applications. Recently, stable ferronematic systems, where the liquid crystal and the magnetic aspects are on equal footing, have drawn increasing attention (apart from other rather exotic phases, like ferrovesicles [46]). Birefringence [47–49] behavior in homogeneous electric [50], and magnetic fields (including the Frederiks transition [48, 51–53]) in inhomogeneous fields [54], and under the influence of bounding surfaces [55] have been investigated.

In their original work Brochard and de Gennes started from the so-called "rigid anchoring" approximation, implying that the directions of the director $\mathbf{n}$ and the local magnetization $\mathbf{M}$ are perfectly co-aligned. However, with the synthesis of thermotropic ferronematics [56] it became evident that the rigid-anchoring approximation might not be generally applicable. Within the

framework of a microscopic model of rod-like ferromagnetic grains Burylov and Raikher [48] reconsidered the surface interaction between the liquid crystalline nematogens and derived an expression for the free energy of a ferronematic.

Apart from the strong response to external magnetic fields that shows up in a possible dependence of all susceptibilities and transport parameters on the square of the field strength, there are additional dynamic effects linear in the field strength [57] . In ordinary nematics those effects are always neglected, but in ferronematics with their strong sensitivity to magnetic fields there is the expectation that these effects are sufficiently enhanced. They can be described as linear-field-dependent additions to ordinary dynamic material tensors describing, for example, heat conduction, diffusion, electric conductivity, viscosity, flow alignment and relaxation of the director. Since a magnetic field is odd under time reversal symmetry, these new effects are reversible (non-dissipative), if the field-free part of the tensor describes a dissipative effect and vice versa. In isotropic systems a few of such effects are known (Hall and Righi-Leduc effect [58]).

The macroscopic description of ferronematics is given in Refs. [57, 59]. The main problem is that the most general form of these equations is too complicated creating problems in the experimental evaluation of the many phenomenological parameters. In such a situation it seems worthwhile to work out some indirect ways to measure the phenomenological parameters. To this goal the investigation of various instabilities can serve as a very convenient tool.

1.4 Scope of this thesis

In chapter 2 we consider the ferrofluid as a binary mixture without an external magnetic field. We show that when we deal with thermal convection instabilities the binary mixture consideration is the appropriate one. This is due to the fact that a rather pronounced Soret effect in combination with very different densities of the magnetic grains and the carrier fluid create a considerable buoyancy force that change the picture of the instability qualitatively. We show that the real threshold of the instability is well bellow the usual value for a one-component liquid. But this threshold is experimentally inaccessible due to the extremely long time scale involved. On the other hand, when we are close to the threshold of the usual one-component convection the effect of the binary mixture nature of ferrofluids shows up on time scales compatible to those in usual thermal convection. Using a simple Galerkin model we describe the nonlinear behavior of our system.

In chapter 3 we consider the thermal convection of ferrofluids in the presence of a magnetic field. To do so we first derive the equations for the binary mixtures in the presence of a magnetic field from most general thermodynamic principles. Then, based on these equations we describe the non-linear behavior of the system using a Galerkin model. The problem is addressed numerically and analytically. By the analytical considerations we show the importance of the boundary layer when a magnetic field is present. Due to this fact the numerical solution becomes more complicated than it was without a magnetic field.

In chapter 4 we consider how linear magnetic field effects appear in different instabilities of ferronematics. We consider Rayleigh-Bénard and Saffman-Taylor instabilities. In both cases we show that these magnetic field effects lead to a qualitatively different picture of these instabilities in ferronematics.

Chapter 2

Thermodiffusion effects in convection of ferrofluids

2.1 Introduction

Thermal convection in binary mixtures has attracted much research activity in the past (see [25–27] for a review). In comparison to the pure fluid case, the dynamics and the bifurcation scenario are more complicated due to the extra degree of freedom associated with the concentration field. Thereby solutal currents are not only driven by concentration gradients, they occur also in response to temperature inhomogeneities. This is denoted as the thermo-diffusive or Soret effect. Its influence on the convective buoyancy force is quantified by the dimensionless separation ratio ψ. The sign of ψ indicates whether temperature- and solutal-induced density gradients are co-aligned $(+)$ or opposed to each other $(-)$. At negative ψ the motionless conductive state experiences an oscillatory instability, saturating in a nonlinear state of traveling waves [27]. On the other hand, at positive ψ the convective instability remains stationary, but the critical Rayleigh number for the onset of convection is dramatically reduced as compared to the pure-fluid reference value $Ra_c^0 = 1708$. This is a result of the joint action of thermal and solutal buoyancy forces. The present paper is dedicated to the case of positive ψ in colloidal suspensions.

A typical property of binary mixture convection is the formation of concentration boundary layers [28]. This is a consequence of the fact that the concentration diffusivity D_c in mixtures is usually much smaller than the heat diffusivity κ. For molecular binary mixtures the dimensionless Lewis number $L = D_c/\kappa$ adopts typical values between 0.1 and 0.01 [60]. If colloidal suspensions are under consideration, the time scale separation is even more dramatic. In this context magneto-colloids, also known as ferrofluids, are a canonical example. These materials are dispersions of heavy solid ferromagnetic grains suspended in a carrier liquid [1]. With a typical diameter of 10 nm the particles are pretty large on molecular length scales, resulting in an extremely small particle mobility. This feature is reflected by Lewis numbers as small as $L = 10^{-4}$ [61]. The smallness of L leads to a situation where separation effects (if any) take place on time scales far beyond any reasonable observation time. Thus, in those experiments, where thermodiffusion is irrelevant, ferrofluids can safely be treated as single-component fluid systems.

However, ferrofluids are also known to exhibit a very large separation ratio ψ. This ob-

servation is due to the pronounced thermo-diffusivity of these materials in combination with the fact that the specific weights of the two constituents (magnetite and water/oil) are quite distinct. Following investigations of Blums et al. [61], who carried out experiments with a thermo-diffusion chamber, ψ can adopt values up to about 100. Recent light scattering investigations of Bacri et al. [23], reveal ψ-values between around -200 (for ionic ferrofluids) and up to $+30$ (cyclohexane carrier) at a volume concentration of 10%. Meanwhile the Soret effect in ferrofluids has also been studied under the influence of an external magnetic field [62–64].

A fairly small number of papers deals with convection in ferrofluids. Most of them treat these liquids as single-component fluids, focusing on the extra drive associated with the temperature dependence of the magnetization (pyro-magnetic effect) [7,8,65]. An experimental study with a binary system of ordinary ψ and L values has been reported some time ago [66]. Quite recently Shliomis and Souhar [11] studied the influence of the concentration field on thermal convection in ferrofluids without an external magnetic field. Using linear arguments they predicted a novel kind of relaxation-oscillation convection to appear at Rayleigh numbers below Ra_c^0. Meanwhile, magnetic field related effects have also been investigated in this problem [67].

The purpose of the present chapter is to work out more closely the role of the concentration field. For the sake of concreteness we phrase the discussion in terms of ferrofluids but point out that the results apply equally well to any binary mixture with small L and large positive ψ [9].

Provided no magnetic field is applied, thermal convection in a perfectly intermixed ferrofluid is usually believed [11] to behave as a single-fluid system. However, our investigation reveals that this is not correct. Rather it is the combination of both, the weak solutal diffusivity and the pronounced solutal buoyancy force, which renders the convective dynamics distinct from the pure fluid case. It will be demonstrated below that a Rayleigh-Bénard setup will become unstable at Rayleigh numbers well below Ra_c^0. Within a time, small compared to the creeping solutal diffusion time, convective perturbations are found to grow up and saturate in a stationary convective state.

The rest of this chapter is organized as follows. In the next section the problem is set up along with the governing equations and boundary conditions. Sec. 2.3 presents a linear analysis specially tailored to account for the slow concentration diffusion. In Sec. 2.4 a Galerkin model is employed for predicting the long time nonlinear convective behavior.

2.2 Setting up the problem

Let us consider a laterally infinite horizontal layer of an incompressible ferrofluid (density ρ, kinematic viscosity ν) bounded by two rigid impermeable plates (see Fig. 2.1). The setup is heated from below with a temperature difference $T_1 - T_0$ between the plates. In the present chapter we do not consider magnetic field related effects, thus the evolution equations for non-magnetic binary mixtures can be adopted. Taking $C(\boldsymbol{r}, t)$ as the concentration of the solid constituent of the suspension, the dimensionless equations for the Eulerian fields of velocity

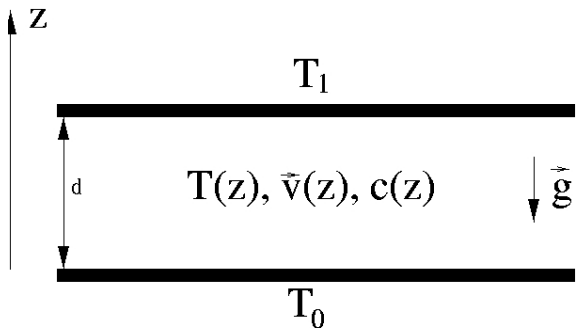

Figure 2.1: Sketch of the setup. For details see text.

$\boldsymbol{v}(\mathbf{r},t)$, temperature $T(\boldsymbol{r},t)$, and $C(\boldsymbol{r},t)$ read in Boussinesq approximation [68–70]

$$\begin{aligned}
\boldsymbol{\nabla}\cdot\boldsymbol{v} &= 0, && (2.1)\\
\partial_t\boldsymbol{v}+\boldsymbol{v}\cdot\boldsymbol{\nabla}\boldsymbol{v} &= -\boldsymbol{\nabla}p+Pr\,\boldsymbol{\nabla}^2\boldsymbol{v}+Pr\,Ra\left[(T-\bar{T})-\psi(C-\bar{C})\right]\boldsymbol{e}_z && (2.2)\\
\partial_t T+\boldsymbol{v}\cdot\boldsymbol{\nabla}T &= \boldsymbol{\nabla}^2 T, && (2.3)\\
\partial_t C+\boldsymbol{v}\cdot\boldsymbol{\nabla}C &= L(\boldsymbol{\nabla}^2 C+\boldsymbol{\nabla}^2 T). && (2.4)
\end{aligned}$$

Here we have scaled length by the layer thickness d, time by the characteristic heat diffusion time h^2/κ, temperature by $\beta_0 d$ ($\beta_0=(T_1-T_0)/d$), and the concentration by $(D_s/D_c)\beta_0 d$. The scale for the pressure p is $\kappa^2\rho/d^2$. Thereby κ, D_c, D_s are the coefficients for heat, concentration and thermo-diffusion, respectively. The quantities $\bar{T}$ and $\bar{C}$ are reference values defined as the mean values for temperature and concentration. Apart from the Prandtl number $Pr=\nu/\kappa$ and the Lewis number $L=D_c/\kappa$ there is a third dimensionless material parameter, the separation ratio $\psi=D_s\alpha_c/(D_c\alpha_\theta)$, where $\alpha_\theta=-(1/\rho)\partial\rho/\partial T$ and $\alpha_c=(1/\rho)\partial\rho/\partial c$ are the thermal and solutal expansion coefficient. The dimensionless Rayleigh number $Ra=\alpha_\theta g d^4\beta_0/(\kappa\nu)$ is the control parameter measuring the strength of the thermal drive. In Eq. (2.4) we have suppressed the Dufour-effect (heat current driven by a concentration gradient) as it is significant in gas mixtures, only.

The equations of motion are to be completed by boundary conditions: Taking the bounding plates to be no-slip for the velocity, highly heat conducting, and impermeable for concentration currents we have at the upper ($z=1/2$) and the lower ($z=-1/2$) plates

$$\begin{aligned}
\boldsymbol{v}|_{z=\pm 1/2} &= 0, && (2.5)\\
T|_{z=\pm 1/2} &= \bar{T}\mp\frac{1}{2}, && (2.6)\\
(\nabla_z C+\nabla_z T)|_{z=\pm 1/2} &= 0. && (2.7)
\end{aligned}$$

Eq. (2.7) guarantees that a concentration current cannot penetrate the plates. Owing to the Soret effect the applied temperature difference enforces a finite concentration gradient at the boundaries. The above equations (2.1)-(2.4) together with the boundary conditions (2.5)-(2.7) complete the system of hydrodynamic equations for the variables $\boldsymbol{v}, T, C$.

2.3 Linear stability analysis

2.3.1 Basic state and time scale separation

It is easy to show that the above boundary-value problem has a simple stationary solution, the so called conductive state. It is represented by linear temperature and concentration distributions

$$\begin{aligned} \boldsymbol{v} &= 0, && (2.8)\\ T_{cond}(z) &= \bar{T} - z, && (2.9)\\ C_{cond} &= \bar{C} + z. && (2.10) \end{aligned}$$

In order to check for the stability of this solution one usually proceeds by introducing small perturbations around the conductive state and following their time evolution as governed by the linearized equations of motion. However, owing to the smallness of the Lewis number, the time necessary to establish C_{cond} exceeds the equilibration time for T_{cond} by a factor $1/L$. Take for instance [11] a layer with a depth of $d = 3$ mm. Then T_{cond} is adopted after a few thermal diffusion times $t_{td} \equiv d^2/\kappa$ ($= 1$ in dimensionless units). With the heat diffusivity of water, $\kappa = 1.5 \times 10^{-7}$ m^2/s, this period amounts to about one minute. On the other hand, for $L = 10^{-4}$ the equilibration of the linear conducting concentration profile C_{cond} takes $d^2/(\kappa L)$, i.e. several days! Clearly, this tops any reasonable time scale at which convection experiments are carried out. Accordingly, a linear stability analysis, suitable for a comparison with experiments, has to account for the creeping solutal diffusivity. This can be accomplished by taking the slowly establishing concentration profile $c_0(z,t)$ as the effective basic state rather than the fully developed profile C_{cond}. For times larger than the evolution time of the temperature profile, $t > t_{td}$, $c_0(z,t)$ obeys the linear partial differential equation

$$\partial_t c_0 = L\nabla_z^2 c_0 \tag{2.11}$$

with the inhomogeneous boundary condition

$$\nabla_z c_0|_{z=\pm 1/2} = 1. \tag{2.12}$$

resulting from Eq. (2.9). On the creeping time scale of the evolution of $c_0(z,t)$, $\tau \equiv Lt$, the validity condition of Eqs. (2.11,2.12) reads $\tau \geq L \simeq 10^{-4}$.

Eqs. (2.11,2.12) reflect the evolution of the upcoming conductive concentration profile C_{cond}. However, as outlined at length above, the system has not enough time to reach this state. At best the Soret driven concentration current is able to pile up thin concentration boundary layers along the plates, the depth δ of which remains small in comparison to the distance between the plates ($\delta \ll 1$). This is somewhat difficult to see from the exact solution of (2.11,2.12)

$$c_0(z,t) = z + \frac{4}{\pi}\sum_{n=0}^{\infty} \frac{(-1)^{n+1}}{(2n+1)^2} \exp\left(-(2n+1)^2\pi^2\tau\right) \sin(2n+1)\pi z \tag{2.13}$$

since for the small τ's we are interested here, the sum converges extremely slowly. A better feeling of c_0 can be obtained by the solution of the somewhat simpler problem where the

boundary conditions (2.12) are replaced by $\nabla_z c_0|_{z=-1/2} = 1$ and $\nabla_z c_0|_{z\gg -1/2} \approx 0$ [11]. The solution of this problem is

$$\nabla_z c_0^{(approx)}(z,t) = 1 - \mathrm{erf}\left(\frac{1/2+z}{2\sqrt{\tau}}\right), \tag{2.14}$$

which for $\tau \gtrsim 10^{-4}$ describes the development of the boundary layer close to $z = -1/2$ very well. ($\mathrm{erf}(x)$ denotes the error function [71].) As long as each boundary layer does not feel the presence of the opposite one, the superposition of (2.14) with the corresponding solution at $z = 1/2$ gives the realistic picture of c_0. We will also corroborate this scenario within the nonlinear calculations below.

2.3.2 Linear deviations

To probe the stability of the ground state, deviations are added whose time evolution is investigated. To that end we impose [72]

$$C(\boldsymbol{r},t) = c_0(z,t) + c(\boldsymbol{r},t), \tag{2.15}$$
$$T(\boldsymbol{r},t) = T_{cond}(z) + \theta(\boldsymbol{r},t), \tag{2.16}$$

and the velocity field $\boldsymbol{v}(\boldsymbol{r},t)$. Linearizing the equations of motion for the convective perturbations $\boldsymbol{v}$, θ, c yields

$$\partial_t \boldsymbol{\nabla}^2 w = PrRa(\nabla_x^2 + \nabla_y^2)[\theta - \psi c] + Pr\boldsymbol{\nabla}^4 w, \tag{2.17}$$
$$\partial_t \theta - w = \boldsymbol{\nabla}^2\theta, \tag{2.18}$$
$$\partial_t c + w\nabla_z c_0 = L[\boldsymbol{\nabla}^2 c + \boldsymbol{\nabla}^2\theta]. \tag{2.19}$$

Here we have taken twice the curl of the Navier-Stokes equation to derive the equation for the vertical component w of the velocity field.

The boundary conditions read as

$$w|_{z=\pm 1/2} = 0, \tag{2.20}$$
$$\nabla_z w|_{z=\pm 1/2} = 0, \tag{2.21}$$
$$\theta|_{z=\pm 1/2} = 0, \tag{2.22}$$
$$(\nabla_z c + \nabla_z\theta)|_{z=\pm 1/2} = 0. \tag{2.23}$$

Eqs. (2.17-2.19) together with (2.20-2.23) are to be solved for a given c_0.

Since the temporal evolution of the boundary layers takes place on the stretched time scale $1/L$ we consider the profile $c_0(z,\tau)$ as being stationary within the period at which convective perturbations grow up to saturation, i.e. $c_0(z,t) \simeq c_0(z)$. The self-consistency of this assumption has to be checked at the end of the calculations. With this approximation of a stationary c_0 all coefficients in Eqs. (2.17-2.19) are time-independent and solutions in the form $\theta, c, w \propto e^{\lambda t}\cos kx$ can be adopted. This leads to

$$\lambda\left(\nabla_z^2 - k^2\right) w = -Pr\,Ra\,k^2(\theta - \psi c) + Pr\left(\nabla_z^2 - k^2\right)^2 w, \tag{2.24}$$
$$\lambda\theta - w = \left(\nabla_z^2 - k^2\right)\theta, \tag{2.25}$$
$$\lambda c + w\nabla_z c_0 = L\left(\nabla_z^2 - k^2\right)(c + \theta). \tag{2.26}$$

Note that the above ordinary differential system is not autonomous since $c_0(z)$ entails an explicit z-dependence. Only in the limiting cases where either $\nabla_z c_0 = 1$ (fully developed conductive concentration profile, i.e., $c_0 = C_{cond}$) or $\nabla_z c_0 = 0$ (uniform concentration distribution), Eqs. (2.24-2.26) adopt an autonomous form. These two situations will be discussed in turn below.

2.3.3 Threshold for a fully developed conductive concentration profile

Although the fully developed conductive profile is of minor significance for the present investigation let us briefly review [26, 27] the situation when $c_0 = C_{cond}$ or equivalently $\nabla_z c_0 = 1$ is the ground state. To identify the threshold of the stationary instability we impose $\lambda = 0$. We obtain $(\nabla_z^2 - k^2)\theta = -w$ from Eq. (2.25) and $(\nabla_z^2 - k^2)c \simeq w/L$ from (2.26), since $L \ll 1$. This allows to neglect thermal vs. solutal buoyancy forces in Eq. (2.24) leading to

$$L\,\left(\nabla_z^2 - k^2\right)^3 c - \psi\, Ra\, k^2\, c = 0 \tag{2.27}$$

with the boundary conditions

$$\nabla_z c|_{z=\pm 1/2} \approx 0 \tag{2.28}$$

$$(\nabla_z^2 - k^2)c|_{z=\pm 1/2} = \nabla_z(\nabla_z^2 - k^2)c|_{z=\pm 1/2} = 0. \tag{2.29}$$

The solution of this eigenvalue problem is known [73] to provide a stationary instability with a critical wave number $k = k_c = 0$ at

$$Ra_c^\infty = 720\,\frac{L}{\psi}. \tag{2.30}$$

Taking $L = 10^{-4}$ and $\psi = 10$ we obtain $Ra_c^\infty \simeq 10^{-2}$, indicating that the threshold of Soret driven convection is smaller by a factor of 10^5 as compared to the pure fluid threshold $Ra_c^0 \simeq 1708$. Note however, that in order to experimentally verify this drastic onset reduction one has to wait for about a week after any temperature step before the linear conductive concentration profile has fully equilibrated. This case will not be pursued further.

2.3.4 Threshold at a uniform concentration distribution

We now turn to the opposite limit when the concentration boundary layer had no time to develop, thus $c_0 = \bar{C}$ or equivalently $\nabla_z c_0 = 0$. Imposing again zero growth rate $\lambda = 0$ we obtain from Eqs. (2.26,2.23) the equality $c = \theta$. Substituting this into (2.24) yields

$$(\nabla_z^2 - k^2)^2 w - Ra\, k^2 (1+\psi)\,\theta = 0, \tag{2.31}$$

$$(\nabla_z^2 - k^2)\theta + w = 0. \tag{2.32}$$

In combination with the boundary conditions (2.20,2.22) we recover the known boundary value problem for pure-fluid thermo-gravitational convection, however with an extra prefactor $(1+$

ψ) in front of the Rayleigh number. Taking this renormalization into account and following Chandrasekhar's solution [74] yields an exchange of stability at

$$Ra_c = \frac{1}{1+\psi} Ra_c^0 \tag{2.33}$$

with a critical wave number $k_c = 3.117$ and $Ra_c^0 \simeq 1708$.

The appreciable value of the separation ratio ψ implies a significant onset reduction. Strictly speaking, the determination of Ra_c by imposing zero growth rate $\lambda = 0$ is void, since the creeping diffusion of c_0 can only be disregarded for times $t \ll L^{-1}$. In other words, the exponential amplification of the *convective* perturbation c has to proceed much faster than the *diffusive* evolution of c_0. This is always true for Rayleigh numbers sufficiently off from Ra_c, i.e., when λ is non-zero with $|\lambda(Ra)| \gg L$. It is this inequality which guarantees the validity of the time scale separation. And it is also the experimentally relevant case because extreme waiting times are circumvented. This situation will be focused on in the following.

2.3.5 Linear growth rate

The preceding discussion reveals that a linear stability theory, suitable to compare with a convection experiment, has to rely on the growth rates of the convective perturbations rather than the threshold value. To that end we assume that the spatial profiles of velocity and temperature are only slightly disturbed by the concentration dynamics. Accordingly we represent their dependencies in terms of simple trigonometric test functions in the form

$$w(x,z,t) = A(t)\cos(kx)\cos^2(\pi z), \tag{2.34}$$
$$\theta(x,z,t) = B(t)\cos(kx)\cos(\pi z). \tag{2.35}$$

In contrast, for the convective concentration field c we allow for a steep boundary layer behavior, which we account for by the following multi-mode expansion

$$c(x,z,t) = -\theta(x,z,t) + \cos(kx)\sum_{n=0}^{n=\infty} b_n(t)\cos(2\pi n z). \tag{2.36}$$

Again we assume that the conductive concentration boundary layers had not enough time to pile up thus imposing $\nabla_z c_0 = 0$. It is easy to see that (2.36) satisfies the boundary conditions (2.7). Furthermore it conserves the mirror symmetry of c with respect to the mid-plane between the boundaries ($z \to -z$). Substituting (2.36) into (2.17-2.19), and projecting the equations with the respective Galerkin modes reveals that only the first two concentration modes b_0 and b_1 enter the evolution equation for A. The remaining concentration modes b_i with $i \geq 2$ are decoupled. Summarizing the Galerkin model for the relevant modes $A(t)$, $B(t)$, $b_0(t)$, $b_1(t)$ leads to the following system of equations

$$
\begin{aligned}
0 &= \frac{3k^2+4\pi^2}{8Pr}\,\lambda A + \left(\frac{3k^4}{8} + k^2\pi^2 + 2\pi^4\right) A \\
&\quad -\frac{4k^2}{3\pi}\,Ra\,(1+\psi)\,B + \frac{\psi k^2}{4}\,Ra\,(2b_0+b_1) && (2.37)\\
0 &= \frac{4}{3\pi}\,\lambda B + \frac{4}{3\pi}(\pi^2+k^2)\,B - \frac{3}{8}\,A && (2.38)\\
0 &= \lambda b_0 + Lk^2\,b_0 + \frac{2(\pi^2+k^2)}{\pi}\,B - \frac{9}{16}A && (2.39)\\
0 &= \lambda b_1 + L(k^2+4\pi^2)\,b_1 + \frac{4}{3\pi}(\pi^2+k^2)\,B - \frac{3}{8}\,A && (2.40)
\end{aligned}
$$

To check the reliability of the above 4-mode approximation we solved the linearized boundary value problem of equations (2.17-2.23) exactly by means of the numerical method outlined in Ref. [75] (cf. App. 2.6.1). Comparing the results for the growth rate λ we found that the Galerkin technique is accurate by about 10%.

For $\lambda \gg L$ and $\psi \gg 1$ (with the approximation $k \approx \pi$) an analytical expression for λ as an implicit function of the material and the control parameters (ψ, L, Pr, and Ra, respectively) can be obtained from Eqs. (2.37-2.40)

$$3Ra\,Pr(\lambda + 2\pi^2 L\psi) = \lambda(2\pi^2+\lambda)(27\pi^2 Pr + 7\lambda). \qquad (2.41)$$

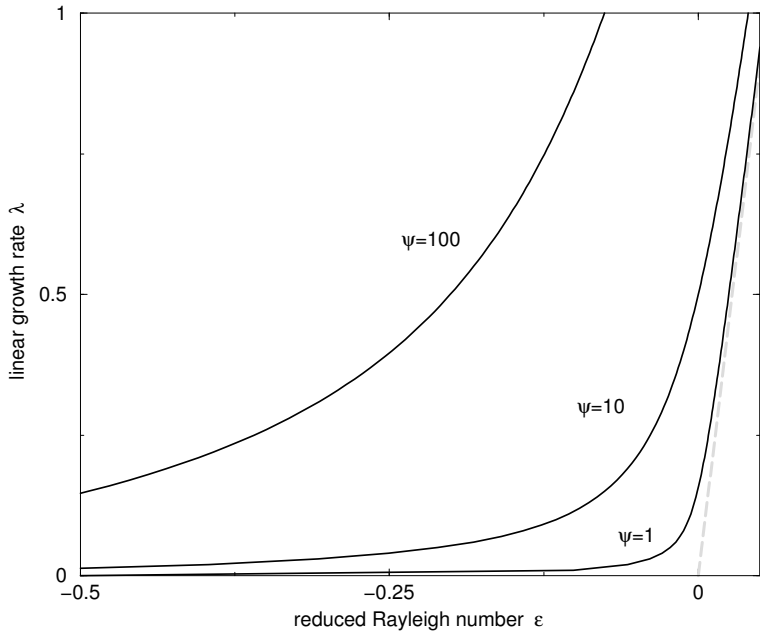

Figure 2.2: The linear growth rate $\lambda\,(\varepsilon)$ for convective perturbations as a function of the reduced Rayleigh number $\varepsilon = Ra/Ra_c^0 - 1$. Here Ra_c^0 is the threshold for the onset of convection in a single-component fluid. Within the present Galerkin approximation $Ra_c^0 = 1752$

Without these approximations numerical results in Fig. 2.2 illustrate the dependence of λ on the reduced Rayleigh number $\varepsilon = Ra/Ra_c^0 - 1$ for different values of the separation ratio. The dashed line bifurcating at $\varepsilon = 0$ indicates the reference case of single-fluid convection. From

Eq. (2.41) and Fig. 2.2 it becomes clear that λ depends for large ψ on the product ψL rather than L alone. Thus decreasing the concentration diffusivity L makes the curve $\lambda(\varepsilon)$ approach to the pure fluid case. On the other hand, increasing the solutal buoyancy force by rising ψ has the opposite effect. Assuming that the experimental observation time is long enough to detect an unstable convective mode with a growth rate $\lambda \simeq 0.1$ (i.e. waiting time of about 10 heat diffusions times, which in a layer of thickness $h = 3$ mm corresponds to about 10 minutes, and which is still much shorter than L^{-1}, the time scale of c_0), then convective motion is detectable at Rayleigh numbers 10-50% below Ra_c^0 depending on the value ψ.

To corroborate the validity of the time scale separation we have also solved the linear problem, where the approximative uniform concentration distribution $\nabla_z c_0 = 0$ was replaced by the true profile as given by Eq. (2.14) at $t = 10$. Re-evaluating the growth rate yields a value for λ which differs from the previous one by less than 10%.

Regarding typical ψ-values in the range $\psi \simeq$ 10-100, Eq. (2.33) indicates that the convective onset threshold Ra_c for a homogeneously intermixed ferrofluid experiences a significant reduction relative to the pure-fluid value Ra_c^0 (cf. Sec. 2.3.4). This result appears somewhat counter-intuitive: As long as the initial concentration profile is approximately uniform, one might expect convection to behave as in single-component liquids [11]. But it turns out here that this argument is not generally applicable: Provided the applied Rayleigh number is not too far below the reference value Ra_c^0, Fig. 2.2 reveals that the *effective* profile $c_0(z, \tau)$ and the *convective* one $c(\boldsymbol{r}, t)$ evolve on strongly distinct time scales. While the former always proceeds on the creeping time scale $1/L$, the quantity $c(\boldsymbol{r}, t)$ grows up much more rapidly proportional to $e^{\lambda t}$, in unison with θ and w. Then, owing to the pronounced ψ-value, solutal buoyancy forces significantly contribute to the destabilization of the conductive state.

Our observations shed new light on a state of relaxation-oscillation convection predicted recently by Shliomis and Souhar [11]. In that paper it was argued that after a sudden application of $Ra < Ra_c^0$ to a ferrofluid with an initial uniform concentration distribution, a concentration boundary layer along the plates piles up slowly, making the instantaneous convective threshold $Ra_c(t)$ gradually sink below the applied Ra-value. Then the increasing convective motion mixes up the ferrofluid, sweeping out the concentration boundary layers. With the concentration profile being re-homogenized, the ferrofluid was argued to behave like a single-component liquid, returning to the conductive state since the applied Rayleigh number is smaller than Ra_c^0. Thereafter this relaxation-oscillation cycle can start again. The present investigation reveals that such a cycle cannot work: This is because it was proven that convective perturbations in a homogeneously mixed ferrofluid do not decay at $Ra_c < Ra < Ra_c^0$. Rather they may experience a considerable positive growth rate (cf. Fig. 2.2) even at Rayleigh numbers 50% *below* Ra_c^0, say. We conclude that there is no mechanism, which drives the system back to the conductive state. Once initiated, convection will persist (rather than oscillate) and saturate in a stationary nonlinear state. This will be shown in the following section.

2.4 Nonlinear behavior

The preceding linear analysis reveals that for Rayleigh numbers well below Ra_c^0, convective fluctuations are exponentially amplified on a time scale, which is experimentally relevant. It can therefore be expected that these fluctuations saturate quickly in a nonlinear convective pattern.

To work out whether this final state is stationary or oscillatory we solved the nonlinear problem by use of numerical methods. To that end we make the following ansatz of a 2-dimensional pattern, which is laterally (in x-direction) periodic with wave number k

$$\begin{aligned} C(x,z,t) &= c_0(z,t) + c(x,z,t) \\ &= c_0(z,t) + c_1(z,t)\cos kx, \qquad (2.42) \\ T(x,z,t) &= T_{cond} + \theta(x,z,t) \\ &= T_{cond} + \theta_0(z,t) + \theta_1(z,t)\cos kx, \qquad (2.43) \\ v_x(x,z,t) &= -(1/k)\nabla_z w_1(z,t)\sin kx, \qquad (2.44) \\ v_z(x,z,t) &= w_1(z,t)\cos kx. \qquad (2.45) \end{aligned}$$

with incompressibility already built in. Substituting (2.42)-(2.45) into the nonlinear equations of motion (2.2-2.4) and sorting for different lateral dependences yields the following system of equations

$$\begin{aligned} \frac{1}{\mathrm{Pr}}\partial_t\left(\nabla_z^2 - k^2\right)w_1 &= \left(D^2 - k^2\right)^2 w_1 - Ra\,k^2\left(\theta_1 - \psi c_1\right), \qquad (2.46) \\ \partial_t c_0 + \frac{1}{2}\nabla_z\left(w_1 c_1\right) &= L\nabla_z^2\left(c_0 + \theta_0\right), \qquad (2.47) \\ \partial_t c_1 + w_1\nabla_z c_0 &= L\left(\nabla_z^2 - k^2\right)\left(c_1 + \theta_1\right), \qquad (2.48) \\ \partial_t\,\theta_0 + \frac{1}{2}\nabla_z\left(w_1\theta_1\right) &= \nabla_z^2\theta_0, \qquad (2.49) \\ \partial_t\,\theta_1 - w_1 + w_1\nabla_z\theta_0 &= \left(\nabla_z^2 - k^2\right)\theta_1, \qquad (2.50) \end{aligned}$$

with the boundary conditions

$$\begin{aligned} \nabla_z\left(c_1 + \theta_1\right)\big|_{z=\pm 1/2} &= 0, \qquad (2.51) \\ \nabla_z\left(c_0 + \theta_0\right)\big|_{z=\pm 1/2} &= 1, \qquad (2.52) \\ \theta_1\big|_{z=\pm 1/2} = \theta_0\big|_{z=\pm 1/2} &= 0, \qquad (2.53) \\ w_1\big|_{z=\pm 1/2} = \nabla_z w_1\big|_{z=\pm 1/2} &= 0. \qquad (2.54) \end{aligned}$$

To solve this boundary-value problem we adopt vertical profiles w_1, θ_0, θ_1, c_0, and c_1 in the form

$$\begin{aligned} w_1(z,t) &= A(t)\cos^2(\pi z), \qquad (2.55) \\ \theta_1(z,t) &= B(t)\cos\pi z, \qquad (2.56) \\ \theta_0(z,t) &= G(t)\sin 2\pi z, \qquad (2.57) \\ c_0(z,t) &= z - \theta_0(z,t) + \sum_{n=0}^{n=N} a_n(t)\sin(2n+1)\pi z, \qquad (2.58) \\ c_1(z,t) &= -\theta_1(z,t) + \sum_{n=0}^{n=N} b_n(t)\cos 2n\pi z, \qquad (2.59) \end{aligned}$$

which satisfy the boundary conditions (2.51-2.54) identically. The above equations describe two-dimensional convection in the form of parallel rolls along the y axis in an infinite slab of

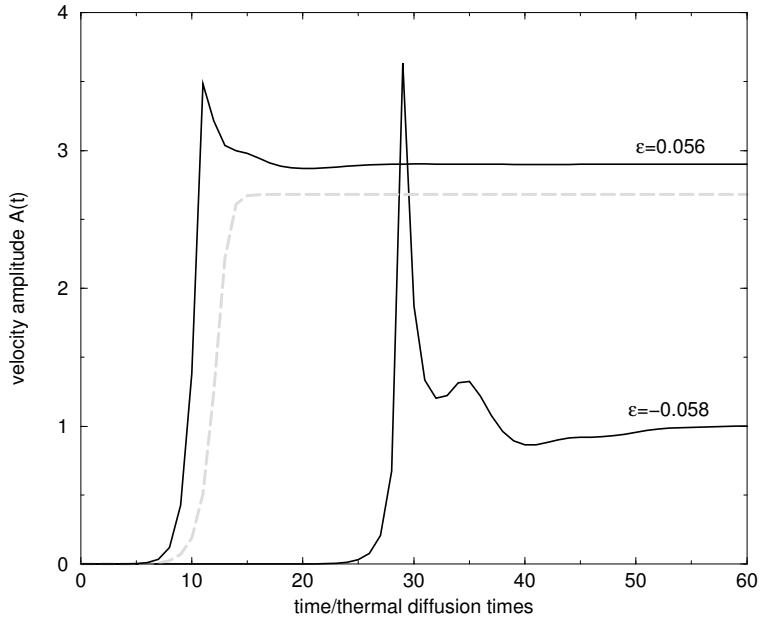

Figure 2.3: The time dependence of the velocity amplitude $A(t)$ for positive and negative values of $\varepsilon = Ra/Ra_c^0 - 1$ in terms of the thermal diffusion time t_{td} (for $Pr = 7$ and $L = 7 \times 10^{-5}$). The dashed gray line corresponds to single-component fluid ($\psi = 0$) $\varepsilon = 0.056$.

thickness 1. We point out that for $\psi = 0$, the concentration fields decouple from temperature and velocity. This reduces Eqs. (2.55-2.57) to the 3-mode model introduced by Lorenz [76] to mimic the dynamics of convective rolls in single-component Rayleigh-Bénard convection. At non-zero ψ, convection is modified by the concentration field but we can adopt the above few-mode expansions for temperature and velocity without modifications, because the diffusivities for heat and momentum are large enough to prevent the appearance of strong gradients. By way of contrast, owing to the small Lewis number, the concentration field does build up steep boundary layers, which we account for by multi-mode Fourier series as given in (2.58,2.59). For c_0 the modes are antisymmetric in z and resemble the solution (2.13), while for c_1 symmetric modes are appropriate. The number N of contributing modes was taken large enough to ensure that the results are insensitive against a further increase of N. For the parameter values considered here, $N = 20$ turned out to be sufficient.

The equations for the mode amplitudes A, B, G, a_n, b_n have been solved by a Runge-Kutta integration. The wave number k, usually taken to be the mode of maximum linear growth rate $\lambda(k, Ra)$ varies between 3 and 3.5 within the investigated Rayleigh number regime. However, since the final predictions of our model turned out not to depend sensitively on the k-value chosen we adopted in all of our simulations $k = \pi$. All runs were started form an initial configuration characterized by a undisturbed linear temperature profile $T = T_{cond}$, a uniform concentration distribution $\nabla_z c_0 = c_1 = 0$, and small random velocity fluctuations. The time evolution of the velocity amplitude $A\,(t)$ as obtained from a typical simulation run is presented in Fig. 2.3 for two different values of the Rayleigh number ($\varepsilon = Ra/Ra_c^0 - 1 = \pm 5.7\%$) on either side of the pure-fluid reference threshold Ra_c^0. The dashed line in Figs.2.3 denotes pure-fluid reference case $\psi = 0$. In all of our runs the convective motion was found to settle in a state

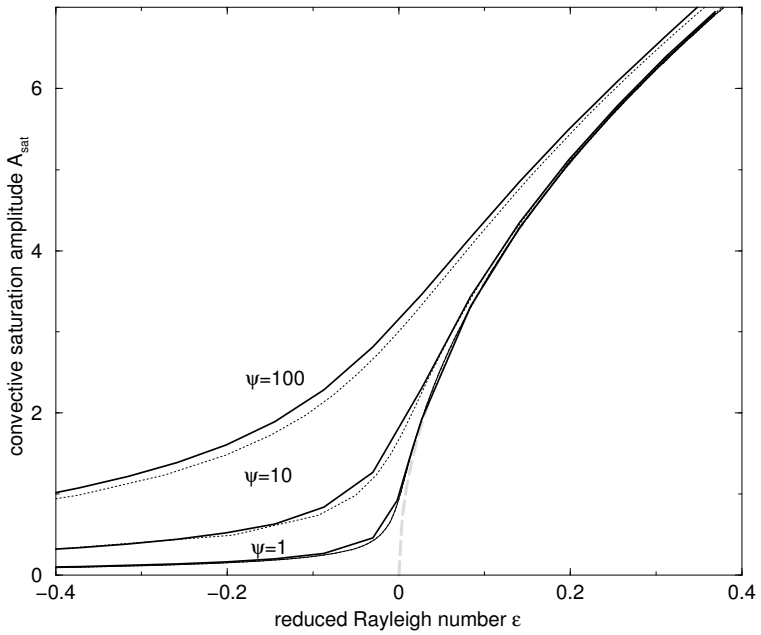

Figure 2.4: The saturation amplitude $A_{sat} = A(t \to \infty)$ as a function $\varepsilon = Ra/Ra_c^0 - 1$ (parameters as in Fig. 2.3). The dashed gray line corresponds to a single-component fluid ($\psi = 0$). Dotted lines show the result of a 7-mode Galerkin approximation as given by Eq.(4.1b) in Ref. [72]

of *stationary* convection. A relaxation oscillation behavior as predicted in Ref. [11] could not be observed. The times necessary to reach the saturation values are several thermal diffusion times and increase with decreasing ε. However, they are still much shorter than the evolution time of the creeping concentration profile, thus corroborating our assumption $\nabla_z c_0 = 0$ in the preceding section. The overshoot in Fig. 2.3 before the plateau values are reached is not a numerical artifact, but it may be related to the small number of lateral modes we have taken into account. This can be expected, since additional modes with negative growth rate, smooth out the relaxation into the saturated state.

Fig. 2.4 shows the corresponding bifurcation diagram with the dependence of the saturation amplitude on the reduced Rayleigh number. At $\varepsilon > 0$ the amplitude saturates at a value, which does not significantly deviate from the single-component case. On the other hand, the influence of the concentration field is most pronounced for $Ra \leq Ra_c^0$. This is a consequence of the competitive interaction between the small Lewis number and the large separation ratio. Decreasing L makes the curve in Fig. 2.4 approach to the dashed reference line, whereas rising ψ has the opposite effect as it amplifies the solutal buoyancy forces. For the sake of comparison the dotted lines in Fig. 2.4 show an analytical approximation for the saturated velocity amplitude based on a seven mode Galerkin approximation recently introduced by Hollinger et al. (Eq. (4.1b) in Ref. [72]).

Unlike a single-component system, where convective perturbations decay for negative ε, the ferrofluid exhibits a pronounced positive linear growth rate (cf. Fig. 2.2). When measuring a bifurcation diagram such as Fig. 2.4, one might conclude that the bifurcation is imperfect. Indeed, a slight imperfect behavior was observed in the experiments of Bigazzi et al. [66] and of

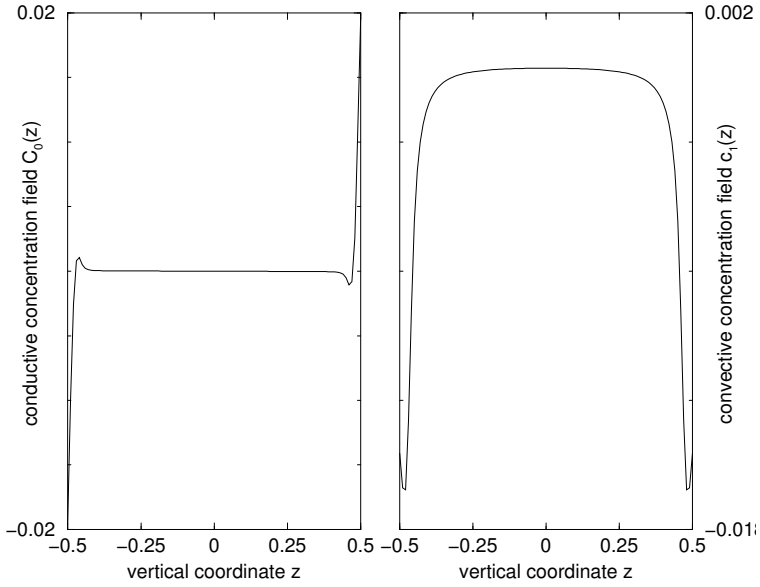

Figure 2.5: (a) The effective concentration profile $c_0(z) = c_0(z, t \to \infty)$ in the fully developed saturated state for $\varepsilon = -0.058$ (parameters $Pr = 7$, $L = 7 \times 10^{-5}$, and $\psi = 10$). (b) same as a) for the amplitude of the convective concentration field $c_1(z) = c_1(z, t \to \infty)$.

Schwab et al. [8], who recorded the convective heat transport as a function of Ra. But we learn here that this phenomenon is to be attributed to the concentration dynamics: As outlined in Sec. 2.3, the very onset for convection is located at a much smaller Rayleigh number, Ra_c, but at Rayleigh numbers slightly larger the linear growth rate of disturbances remains extremely small. Thus, trying to detect Ra_c in such an experiment would be hopeless as it requires extremely long observation times. Experiments on ferrofluids have been reported recently [77] that corroborate the behavior shown in Fig. 2.4.

In contrast, at ε around $\pm$10-20% the time necessary to wait for the equilibration of the nonlinear convective state amounts to only a few *thermal* diffusion times (cf. Fig. 2.3). This statement, which holds in particular also for the concentration field, demonstrates that the growth of convective perturbations is a fast process on the (creeping) time scale $1/L$ of solutal diffusion. On the first view this might appear counterintuitive, but it can be seen from Fig. 2.5 that the final concentration distribution differs from the initial homogeneous profile only in *thin* boundary layers. Consequently, time consuming redistribution processes of the concentration field are not necessary for building up the solutal saturation profiles. This keeps the equilibration time small and no further evolution on the slow diffusion timescale occurs after the system reaches the state given on the Fig. 2.5.

2.5 Conclusions (Chap. 2)

Thermo-convection of binary mixtures with a weak concentration diffusivity and a large separation number has been investigated theoretically. By considering the classical Rayleigh Bénard setup it is shown that both the linear as well as the nonlinear convective behavior is significantly

altered by the concentration field as compared to single-component systems. Starting from an initial motionless configuration with a uniform concentration distribution, convective perturbations are found to grow even at Rayleigh numbers well below the threshold Ra_c^0 of pure-fluid convection. It turned out that the actual critical Rayleigh number Ra_c is drastically smaller, but experimentally inaccessible due to the extremely slow growth of convection patterns for $Ra \gtrsim Ra_c$, requiring extremely large observation times. On the other hand, operating the ferrofluid convection experiment at Rayleigh numbers $Ra_c < Ra \lesssim Ra_c^0$, reveals considerable positive growth rates, which lead to a saturated nonlinear state almost as fast as pure-fluid convection does at $Ra > Ra_c^0$. This result is corroborated by earlier convection experiments. It does not comply with a recent prediction of convective self-oscillations conjectured from the interplay between short thermal and slow solutal diffusion time scales.

2.6 Appendix (Chap. 2)

2.6.1 A method to solve linear stability problems in a fluid layer

In this appendix we describe the method suggested in [75]. The notation in this appendix is mainly independent of the rest of the thesis and corresponds to that used in [75].

Let us consider the following $2n \times 2n$ linear differential system on the z interval $(0, 1)$ with mixed boundary value conditions:

$$\frac{d\boldsymbol{x}}{dz} = A(\boldsymbol{\sigma})\boldsymbol{x} \tag{2.60}$$

$$x_i(0) = 0 \quad \text{for} \quad i = 1, ..., n \tag{2.61}$$

$$x_i(1) = 0 \quad \text{for} \quad i = 1, ..., n \tag{2.62}$$

where $\boldsymbol{x} = [x_1, x_2, ..., x_{2n}]$ and $A(\boldsymbol{\sigma}) = A(\sigma_1, ..., \sigma_k)$ is a given $2n \times 2n$ matrix depending on k parameters σ_i. The problem is to determine the values those parameters that the above system is solvable. Assume the problem has a nontrivial solution $\boldsymbol{x}(z)$ for a given $\boldsymbol{\sigma}$ with

$$\boldsymbol{x}(0) = \boldsymbol{x}_0 = [0, ..., 0, u_1, ..., u_n], \tag{2.63}$$

then we have

$$\boldsymbol{x}(z) = \exp(A(\boldsymbol{\sigma}))\boldsymbol{x}_0 \tag{2.64}$$

Let us write $\exp(A(\boldsymbol{\sigma}))$ in the form of a block matrix

$$\exp(A(\boldsymbol{\sigma})) = \begin{bmatrix} * & E(\boldsymbol{\sigma}) \\ * & * \end{bmatrix} \tag{2.65}$$

with four $n \times n$ matrixes, $E(\boldsymbol{\sigma})$and three others denoted by stars, which we do not need. Then from (2.62)

$$E(\boldsymbol{\sigma})\boldsymbol{u} = E(\boldsymbol{\sigma})[u_1, ..., u_n] = 0. \tag{2.66}$$

In order to have a nontrivial solution of the boundary value problem (2.60-2.62) we need to have a nontrivial solution of Eq. (2.66), consequently

$$\det(E(\boldsymbol{\sigma})) = 0. \tag{2.67}$$

Thus we can conclude, the necessary and sufficient condition for the existence of nontrivial solutions of (2.60-2.62) is $\det(E(\boldsymbol{\sigma})) = 0$. Furthermore, the number of linearly independent solutions equals the dimension of the null space of $E(\boldsymbol{\sigma})$.

The next step is to get the critical characteristic values. The above analysis shows that the characteristic values are simply the solutions of the algebraic equation (2.67), easily obtainable using some standard numerical method such as the Newton-Raphson method. In thermal convection problems, however we are interested in finding the *critical* or minimal ones among these values, e.g. the critical Rayleigh number. Generally, if we want to find the minimum characteristic value for the first parameter σ_1, our problem can be formulated as a constrained optimisation problem:

$$\text{Minimize } \sigma_1, \text{subject to} \det(E(\boldsymbol{\sigma})) = 0.$$

Many subroutines are available for solving this constrained nonlinear programing problem. One may first convert this constrained problem to an unconstrained one by introducing a penalty term in the objective function, then apply unconstrained optimization subroutines.

In [75] it is argued that the following approach is robust for thermal convection problems. The equation

$$f(\sigma) \equiv \det(E(\boldsymbol{\sigma})) = 0 \tag{2.68}$$

generally defines a function $\sigma_1 = \sigma_1(\sigma_2, ..., \sigma_k)$. At the critical value σ_1^* we have

$$\frac{\partial \sigma_1}{\partial \sigma_i} = 0, \qquad i = 2, ..., k. \tag{2.69}$$

and implicit differentiation gives

$$\frac{\partial f}{\partial \sigma_i} = 0, \qquad i = 2, ..., k. \tag{2.70}$$

Thus, the critical value of σ_1 can be found by solving the system of k equations (2.68,2.70).

2.6.2 The piecewise approximation of the non-uniform concentration profile

We cannot straightforwardly apply the method described in the previous section to investigate the stability of binary mixtures at small times, when the concentration profile is not linear. This is because the method described can only be applied to a homogeneous system of differential equations. In order to apply this method we make a piecewise representation of the non-uniform concentration profile:

$$\nabla_z c_0(z,t) = \begin{cases} 1 & \text{if } -1/2 < z < -1/2 + \delta(t) \\ 0 & \text{if } -1/2 + \delta(t) < z < 1/2 - \delta(t) \\ 1 & \text{if } 1/2 - \delta(t) < z < 1/2 \end{cases} \tag{2.71}$$

where $\delta(t) = 2\sqrt{Lt/\pi}$ is the effective boundary layer depth chosen in such a way that the integral of the model function (2.71) is equal to the one taken with function (2.14). The time dependence in (2.71) is considered to be quasi-stationary.

If we now use the concentration profile (2.71) we get a piecewise homogeneous system of differential equations and the final exponent of the matrix (2.64) will be a product of three exponents corresponding to the three intervals of (2.71).

Such an analysis has shown that we can simply put $\delta = 0$ without significant losse of any reasonable accuracy. The error introduced by puting $\delta = 0$ is less then 10%, when the boundary layer is $\delta = 0.1$, that corresponds to a time interval $t \sim 100$.

Chapter 3

The influence of a magnetic field on the Soret-dominated thermal convection in ferrofluids

3.1 Introduction

In this chapter we extend the investigation done in previous one to consider the influence of an external magnetic field on this convection scenario for positive separation ratio ψ [10]. We first (Sec. 3.2) review the hydrodynamic equations for binary mixtures in the presence of an external magnetic field. We assume the magnetization to be already relaxed to its equilibrium value on the time scales under consideration. The magnetic field effects then come basically in two different varieties. First, the Maxwell stress that can be written as a Kelvin force in the momentum conservation law (the Navier-Stokes equation), and second the temperature and concentration dependence of the magnetic susceptibility in the statics that gives rise to a field dependence of heat and concentration currents (magnetophoresis). If a temperature gradient is applied across the ferrofluid layer, as in the case without field [9], the experimentally relevant convection free ground state is not the true stationary state with a linear concentration profile, but the purely conducting state with a constant concentration (apart from a very thin boundary region) in addition a linear magnetic field profile is present in the convection free state (Sec. 3.3). The stability of this ground state is investigated by solving approximately the nonlinear dynamic equations for deviations from it. Within the usual Boussinesq approximation five magnetic field effects, characterized by dimensionless numbers proportional to the field strength squared, show up in the equations and boundary conditions (Sec. 3.4). Among them, M_1 the strength of the magnetic relative to buoyancy force, and M_2, the magnetophoretic number seem to be the most important.

To solve the system of equations we first set up a multi-mode Galerkin description (Sec. 3.5), where in particular for the concentration and the magnetic potential the inclusion of many modes turn out to be essential. An approximate ansatz is solved analytically (Sec. 3.6). Here the necessity of dealing carefully with the boundary layer profiles of concentration and magnetic potential (Apps. 3.9.1 and 3.9.2) becomes obvious. This approximate analytical solution is compared with the numerical Galerkin results, in particular with respect to the influence of the Kelvin force (M_1) in Sec. 3.7. The role of magnetophoresis (M_2) on the instability behavior is

discussed in Sec. **??**.

3.2 Basic equations

Ferrofluids can be treated as super-paramagnetic continuum [1] that consists of two different non-reacting material (binary mixture). An external magnetic field induces easily a considerable magnetization in the fluid. This magnetization is in principle a dynamic degree of freedom. However, it relaxes rather quickly to its equilibrium value and orientation given by the Maxwell field $\boldsymbol{H}$. Thus, for the time scales of interest for the convection problem we can always assume $\boldsymbol{M} = \boldsymbol{M}(\boldsymbol{H})$. Here we review the hydrodynamic equations for a binary mixture subject to an external static magnetic field and bring it into a form suitable for the convection problem. Hydrodynamics is most easily set up by using those quantities as dynamic variables that are related to local conservation laws [78]. In our case that are density ρ, momentum density $\rho\boldsymbol{v}$, entropy density σ and concentration C (of magnetic particles), while the chemical potential μ, the velocity $\boldsymbol{v}$, the temperature T, and the relative chemical potential μ_c are taken as their thermodynamic conjugate quantities, respectively. The dynamic equations read [78]

$$\partial_t \rho + \mathrm{div}(\rho \boldsymbol{v}) = 0 \tag{3.1}$$

$$\partial_t \sigma + \boldsymbol{v}\cdot\boldsymbol{\nabla}\sigma = \boldsymbol{\nabla}\cdot\tilde{\kappa}\,\boldsymbol{\nabla}T + \boldsymbol{\nabla}\cdot\tilde{D}_T\boldsymbol{\nabla}(\frac{\mu_c}{\rho}) + \frac{R}{T} \tag{3.2}$$

$$\rho(\partial_t C + \boldsymbol{v}\cdot\boldsymbol{\nabla}C) = \boldsymbol{\nabla}\cdot D\,\boldsymbol{\nabla}(\frac{\mu_c}{\rho}) + \boldsymbol{\nabla}\cdot\tilde{D}_T\boldsymbol{\nabla}T \tag{3.3}$$

$$\rho(\partial_t v_i + v_j\nabla_j v_i) + \nabla_i p = \nabla_j \rho\,\nu_{ijkl}\nabla_l v_k + M_j\nabla_i H_j + \rho g_i \tag{3.4}$$

while the magnetic field $\boldsymbol{H}$ and induction $\boldsymbol{B}$ are determined by Maxwell's equations, which read in the static and non-conducting case

$$\nabla\cdot\mathbf{B} = 0 \tag{3.5}$$

$$\nabla\times\mathbf{H} = 0 \tag{3.6}$$

Generally, due to the presence of an external field, the transport coefficients $\tilde{\kappa}$, $\tilde{D}_T$, and D should be written as tensors of the form $D_{ij} = D\delta_{ij} + D^R\epsilon_{ijk}H_k$ with Hall- or Righi-Leduc type contributions [57]. However, those terms are inoperative for the geometry considered below. The same is true for similar linear field contributions to the viscosity tensor [57], which can change qualitatively the patterns in the Benard instability in ferronematics [79], but do not contribute here.

As usual for convection problems we apply the Boussinesq approximation implying incompressibility $\mathrm{div}\boldsymbol{v} = 0$, neglection of the dissipation function R in (3.2), and taking all material parameters as constants except for the density in the gravity force ρg_i. The Navier-Stokes equation (3.4) has been written in the form that the Kelvin force, with $\boldsymbol{M} = \boldsymbol{B} - \boldsymbol{H}$ [80], shows up on the right hand side. Due to the incompressibility approximation the pressure p is no longer a thermodynamic variable and its dependence on the magnetic field is irrelevant. It is only an auxillary quantity that ensures the incompressibility condition for all times, but it is not needed in the following. As discussed above, the magnetization is no dynamic degree of freedom.

To close the system of equations we need the static relations between the conjugate quantities and the variables. Standard procedure gives [78]

$$\delta T = \frac{T}{c_V}\delta\sigma + \beta_c\,\delta C \tag{3.7}$$
$$\delta\mu_c = \tilde{\gamma}\,\delta C + \beta_c\,\delta\sigma \tag{3.8}$$
$$\delta\boldsymbol{B} = (1+\chi)\,\delta\boldsymbol{H} \tag{3.9}$$

derived from an energy density

$$\epsilon = \epsilon_0 + \frac{T}{2c_V}(\delta\sigma)^2 + \beta_c(\delta\sigma)(\delta C) + \frac{\tilde{\gamma}}{2}(\delta C)^2 + \frac{1}{2}(1+\chi)(\delta\boldsymbol{H})^2 \tag{3.10}$$

In this form the static equations generally are not suitable for ferrofluids, since the magnetic susceptibility χ depends considerably on the concentration (of the magnetic particles), the temperature and the external field. Switching to the temperature as variable by a Legendre transformation, $\tilde{\epsilon} = \epsilon - (\delta\sigma)(\delta T)$, and taking $\chi = \chi(T, C, H^2)$ we get

$$\delta\sigma = \frac{c_H}{T}\delta T - \frac{\beta_H c_V}{T}\delta C + \chi_T\,\boldsymbol{H_0}\cdot\delta\boldsymbol{H} \tag{3.11}$$
$$\delta\mu_c = \gamma_H\,\delta C + \frac{\beta_H c_V}{T}\delta T + \chi_c\,\boldsymbol{H_0}\cdot\delta\boldsymbol{H} \tag{3.12}$$
$$\delta\boldsymbol{B} = (1+\chi_0)\,\delta\boldsymbol{H} + \boldsymbol{H}_0\,(\chi_T\,\delta T + \chi_c\,\delta C + \chi_H\boldsymbol{H}_0\cdot\delta\boldsymbol{H}) \tag{3.13}$$

where χ_0 is the (constant) magnetic susceptibility taken at the equilibrium field $\boldsymbol{H}_0$, equilibrium temperature T_0, and equilibrium concentration c_0. It is assumed to be a known function of H_0^2. Up to second order derivatives of χ we have

$$c_H = c_V - \frac{T_0}{2}H_0^2\,\frac{\partial^2\chi}{\partial T^2} \tag{3.14}$$
$$\beta_H = \beta_c + \frac{T_0}{2c_V}H_0^2\,\frac{\partial^2\chi}{\partial T\,\partial C} \tag{3.15}$$
$$\gamma_H = \tilde{\gamma} - \frac{\beta^2 c_V}{T_0} + \frac{1}{2}H_0^2\,\frac{\partial^2\chi}{\partial C^2} \tag{3.16}$$
$$\chi_T = \frac{\partial\chi}{\partial T} + H_0^2\frac{\partial^2\chi}{\partial T\,\partial H^2} \tag{3.17}$$
$$\chi_c = \frac{\partial\chi}{\partial c} + H_0^2\frac{\partial^2\chi}{\partial C\,\partial H^2} \tag{3.18}$$
$$\chi_H = 4\frac{\partial\chi}{\partial H^2} + 2H_0^2\frac{\partial^2\chi}{(\partial H^2)^2} \tag{3.19}$$

implying a H_0^2 dependence of the usual static susceptibilities. In principle, the static susceptibilities can be arbitrary functions of H_0^2. Thermodynamic stability (positivity of the energy functional) requires the following positivity conditions

$$\begin{aligned} &c_H > 0, \qquad \gamma_H > 0, \qquad 1+\chi_0 > 0, \qquad \bar{\epsilon} > 0, \\ &c_H\gamma_H > (\frac{\beta_H c_V}{T})^2, \qquad c_H\bar{\epsilon} > \chi_T^2 H_0^2, \qquad \gamma_H\bar{\epsilon} > \chi_c^2 H_0^2, \end{aligned} \tag{3.20}$$

with $\bar{\epsilon} = 1 + \chi_0 + \chi_H H_0^2$ [81].

In order to retain the buoyancy force, the temperature and concentration dependence of the density has to be kept in the gravity force, which can be written as

$$\rho g_i = -g\rho_0(1 + \alpha_\theta\,\delta T - \alpha_c\,\delta C - \alpha_H \boldsymbol{H}_0 \cdot \delta\boldsymbol{H})\,\delta_{iz} \tag{3.21}$$

taking the z direction as the vertical one. The magnetic field contribution to the buoyancy force due to deviations of the magnetic field from its constant and homogeneous equilibrium value has been introduced for completeness.

Combining the static and dynamic part the basic equations are

$$\begin{aligned}
\mathrm{div}\boldsymbol{v} &= 0 && (3.22)\\
(\partial_t + \boldsymbol{v}\cdot\boldsymbol{\nabla})(\frac{c_H}{T_0}T + \chi_T \boldsymbol{H}_0\cdot\boldsymbol{H}) &= \bar{\kappa}\Delta T + \bar{D}_T\frac{\gamma_H}{\rho_0}\Delta C + \bar{D}_T\frac{\chi_c}{\rho_0}\boldsymbol{H}_0\cdot\Delta\boldsymbol{H} && (3.23)\\
\rho_0(\partial_t + \boldsymbol{v}\cdot\boldsymbol{\nabla})C &= D\frac{\gamma_H}{\rho_0}\Delta C + \bar{D}_T\Delta T + D\frac{\chi_c}{\rho_0}\boldsymbol{H}_0\cdot\Delta\boldsymbol{H} && (3.24)\\
(\partial_t + \boldsymbol{v}\cdot\boldsymbol{\nabla})(\mathrm{curl}\boldsymbol{v})_i &= \epsilon_{ikz}g(\alpha_\theta\nabla_k T + \alpha_c\nabla_k C + \alpha_H\boldsymbol{H}_0\cdot\nabla_k\boldsymbol{H}) && (3.25)\\
&+ \frac{1}{\rho_0}\epsilon_{ikl}(\boldsymbol{H}_0\cdot\nabla_l\boldsymbol{H})\,(\chi_T\nabla_k T + \chi_c\nabla_k C) + \nu\Delta(\mathrm{curl}\boldsymbol{v})_i
\end{aligned}$$

with $\Delta = \boldsymbol{\nabla}^2$ and

$$\begin{aligned}
\bar{\kappa} &= \tilde{\kappa} + 2\tilde{D}_T\,\frac{\beta_H c_V}{\rho_0 T_0} + D\big(\frac{\beta_H c_V}{\rho_0 T_0}\big)^2 && (3.26)\\
\bar{D}_T &= \tilde{D}_T + D\,\frac{\beta_H c_V}{\rho_0 T_0} && (3.27)
\end{aligned}$$

The temperature conduction coefficient is $\kappa \equiv \bar{\kappa}T_0/c_H$, the diffusion coeffient $D_c \equiv D\gamma_H/\rho_0^2$, the Soret coefficient is $D_s \equiv \bar{D}_T/\rho_0$, the Dufour coefficient is $D_f \equiv \bar{D}_T\gamma_H T_0/(\rho_0 c_H)$, while ν is the dynamic shear viscosity.

The boundaries are assumed to be ideal thermal conductors, thus the temperature of the fluid at the boundaries is identical to the applied temperature. Note that in real experimental situations the finite heat conductivity of the boundaries could lead to some noticeable effects [65], but we are not going to discuss these effects in what follows. For the velocity field we assume 'rigid' boundary conditions, while for the magnetic field and magnetic induction the usual continuity conditions apply

$$\begin{aligned}
\hat{\mathbf{n}}\cdot(\mathbf{B}_{int} - \mathbf{B}_{ext}) &= 0 && (3.28)\\
\hat{\mathbf{n}}\times(\mathbf{H}_{int} - \mathbf{H}_{ext}) &= 0 && (3.29)
\end{aligned}$$

with $\hat{\boldsymbol{n}}$ the normal of the boundaries. For the concentration of the ferroparticles we have the impermeability condition, i.e. no flux on the boundaries is allowed

$$D\gamma_H\,\hat{\boldsymbol{n}}\cdot\boldsymbol{\nabla}C + \rho_0\bar{D}_T\,\hat{\boldsymbol{n}}\cdot\boldsymbol{\nabla}T + D\chi_c\,\boldsymbol{H}_0\cdot(\hat{\boldsymbol{n}}\cdot\boldsymbol{\nabla})\boldsymbol{H} = 0 \tag{3.30}$$

3.3 Heat conducting state

For a layer of thickness d with prescribed temperatures T_0 and T_1 at the boundaries $z = -d/2,\ d/2$, respectively, and with infinite lateral dimensions the pure conductive state is easily found. The concentration and the magnetic field show linear $z-$deviations from the equilibrium values, given by the boundary conditions (3.28,3.30)

$$\mathbf{v} = 0 \tag{3.31}$$
$$T = \bar{T} - \beta_0 z \tag{3.32}$$
$$C = \bar{C} + \frac{D_1}{D_2}\beta_0 z \tag{3.33}$$
$$H_z = H_0(1 + \frac{D\gamma_H\chi_T - \rho_0\chi_c\bar{D}_T}{\bar{\epsilon}D_2}\beta_0 z) \tag{3.34}$$

where $\beta_0 = (T_0 - T_1)/d$, H_0 is related to the strength of the magnetic field outside the layer $\boldsymbol{H}_{ext}$ by the expression $\boldsymbol{H}_{ext} = (H_0 + M(H_0))\,\hat{\boldsymbol{e}}_z$, and $D_2 = D\gamma_H(1 + O(H_0^2))$. The quantities $\bar{T}$ and $\bar{C}$ are reference values defined as the mean values for temperature and concentration. However, as was the case of thermal convection without magnetic field [9], to reach this conductive state one needs to wait until the very slow process of concentration diffusion has equilibrated. As it was estimated in [9] this takes as long as a week under usual experimental conditions. For this reason we consider the stability not of the state given by Eq. (3.33) but of the quasi-stationary state when the temperature field, Eq. (3.32), is equilibrated, but the concentration field is still homogeneous except for very thin boundary layers near the boundaries. This situation is similar to that without magnetic field considered in [9]. With such an approximation the quasi-stationary state reads

$$\mathbf{v} = 0 \tag{3.35}$$
$$T = \bar{T} - \beta_0 z \tag{3.36}$$
$$C = \bar{C} \tag{3.37}$$
$$H_z = H_0(1 + \frac{\chi_T}{\bar{\epsilon}}\beta_0 z) \tag{3.38}$$

This state is not a solution with the boundary condition (2.7), but it gives a good approximation to the solution for experimentally relevant times.

3.4 Deviations from the conducting state

The next step is to write the equations for the deviations from the heat conducting state (3.35)-(3.38). To do so in dimensionless form we introduce characteristic scales: d for length, d^2/κ for time (with $\kappa = \bar{\kappa}T_0/c_H$), $\beta_0 d$ for temperature, $\beta_0\bar{D}_T\rho_0 d/(D\gamma_H)$ for concentration, κ/d for velocity, and $\beta_0 d\chi_T H_0/\bar{\epsilon}$ (with $\bar{\epsilon} \equiv 1 + \chi_0 + \chi_H H_0^2$) for magnetic field. For the deviations from the magnetic field (3.38) a scalar potential can be introduced $\boldsymbol{H} = H_z\hat{\boldsymbol{e}}_z - \boldsymbol{\nabla}\phi$, while the magnetic potential outside the layer is defined by $\boldsymbol{H}_{ext} = \boldsymbol{H}_0^{ext} - \boldsymbol{\nabla}\phi_e$. The deviation of the

temperature from Eq. (3.36) is θ. Then Eqs. (3.5), and (3.22)-(3.26) lead to

$$\begin{aligned}
\nabla \cdot \mathbf{v} &= 0 && (3.39)\\
[\partial_t + (\mathbf{v}\cdot\nabla)]\,(\theta - M_4\nabla_z\phi) &= w(1-M_4) + \Delta\theta + F\Delta(C - M_2\nabla_z\phi) && (3.40)\\
[\partial_t + (\mathbf{v}\cdot\nabla)]\,C &= L\Delta(\theta + C - M_2\nabla_z\phi) && (3.41)\\
\frac{1}{Pr}\,[\partial_t + (\mathbf{v}\cdot\nabla)]\,(curl\mathbf{v})_i &= Ra\,\epsilon_{ikz}\nabla_k\,[(1+M_1)\,\theta - (\psi + \psi_m M_1)\,C + (M_5 - M_1)\nabla_z\phi] \\
&\quad -Ra\,M_1\,\epsilon_{ikl}(\nabla_l\nabla_z\phi)\nabla_k\,(\theta - \psi_m C) + \Delta(curl\mathbf{v})_i && (3.42)\\
(\nabla_z^2 + M_3\Delta_\perp)\phi &= \nabla_z(\theta - \psi_m C) && (3.43)\\
\Delta\phi_e &= 0 && (3.44)
\end{aligned}$$

where w is the z component of the velocity. The transverse Laplacean $\Delta_\perp = \Delta - \nabla_z^2$. The non-dimensional parameters introduced here are: the Rayleigh number $Ra = \alpha_\theta\beta_0 g d^4/(\kappa\nu)$, the Prandtl number $Pr = \nu/\kappa$, the separation ratio $\psi = \alpha_c\rho_0\bar{D}_T/(\alpha_\theta\gamma_H D)$, the magnetic separation ratio $\psi_m = -\chi_c\rho_0\bar{D}_T/(\chi_T\gamma_H D)$, the Lewis number $L = \gamma_H c_H D/(\rho_0^2\bar{\kappa}T_0) = D_c/\kappa$, the strength of magnetic force relative to buoyancy $M_1 = \beta_0\chi_T^2 H_0^2/(\rho_0 g\alpha_\theta\bar{\epsilon})$, the magnetophoretic number $M_2 = D\chi_c\chi_T H_0^2/(\rho_0\bar{D}_T\bar{\epsilon})$, the nonlinearity of magnetization $M_3 = (1+\chi_0)/\bar{\epsilon} \approx 1 - \chi_H H_0^2/(1+\chi_0)$, the relative strength of the temperature dependence of the magnetic susceptibility $M_4 = \chi_T^2 H_0^2 T_0/(c_H\bar{\epsilon})$, the ratio of magnetic to thermal buoyancy $M_5 = \alpha_H\chi_T H_0^2/(\alpha_\theta\bar{\epsilon})$, and the Dufuor number $F = \bar{D}_T^2/(D\bar{\kappa}) = D_s D_f/(\kappa D_c)$. The stability conditions (3.20) require $M_4 < 1$ and $M_2\psi_m > -1$.

According to our choice of 'rigid' and ideally conducting boundaries, the boundary conditions for the deviations from the conducting state read

$$\begin{aligned}
\theta\,|_{z=\pm\frac{1}{2}} &= 0 && (3.45)\\
w\,|_{z=\pm\frac{1}{2}} &= 0 && (3.46)\\
\nabla_z w\,|_{z=\pm\frac{1}{2}} &= 0 && (3.47)\\
\nabla_z(\theta + C - M_2\nabla_z\phi)\,|_{z=\pm\frac{1}{2}} &= 1 - M_2 && (3.48)
\end{aligned}$$

and the magnetic boundary conditions (3.28), (3.29) are

$$\begin{aligned}
\bar{\epsilon}(\nabla_z\phi + \psi_m C) - \nabla_z\phi_e\,|_{z=\pm\frac{1}{2}} &= 0 && (3.49)\\
\boldsymbol{\nabla}_\perp\phi - \boldsymbol{\nabla}_\perp\phi_e\,|_{z=\pm\frac{1}{2}} &= 0 && (3.50)
\end{aligned}$$

These boundary conditions close the problem to find the fields $\mathbf{v}, \theta, C$, ϕ and ϕ_e.

3.5 Simple Galerkin solution

The set of equations derived in the previous section is still unnecessarily complicated. We will simplify it first by neglecting the Dufour effect, i.e. putting $F = 0$, as is usually done for any liquid. Second we discard M_4, which is a common simplification in the description of instabilities in ferrofluids [7, 82]. Since M_4 is not related to concentration effects, which we are interested in here, we expect not to loose any reasonable aspect of the problem under

consideration. The same is true for the coefficient M_5. It may be important in a situation, where the concentration dynamics is not considered at all, since in that case it is the only non thermal contribution to buoyancy. Thus, we are left with 3 magnetic field dependent effects characterized by $M_{1,2,3}$. The first denotes the influence of the Kelvin force and is expected to have the dominant influence on the convection behavior. The second effect, which we will treat in a second step, constitutes magnetophoresis, the dependence of the concentration current on the magnetic field. The third effect is due to the nonlinearity of the magnetization as a function of the external field. Generally, M_3 is rather close to 1 (the linear case $\chi = const.$ or $\boldsymbol{M} \sim \boldsymbol{H}$), since the dependance on the M_3 is rather weak we always take $M_3 = 1.1$. The parameter ψ is known to be between 10 and 100 and can have negative or positive sign depending on the ferrofluid used [23]. Here we consider only the case of the positive value of ψ. Making a simple estimate we find that the value ψ_m has the same sign and is of the same order of magnitude as ψ for typical ferrofluids.

The boundary value problem obtained in this way is still too complicated to allow a simple analytical (1-mode solution), even if for the velocity field unrealistic 'free' boundary conditions are used. This is due to the magnetic boundary condition (3.49) that involves the concentration. Sacrificing this condition, however, would change the bifurcation scenario qualitatively rendering such an analytical solution worthless. Instead, any realistic treatment has to take into account the boundary layer fields of concentration and magnetic field potential. We will do this analytically later on in a simplified way guided by the numerical results, which we will derive first using the Galerkin technic. To that end we make the following ansatz of a 2-dimensional pattern, which is laterally (in x direction) infinite and periodic with wave number k. These equations describe two-dimensional convection in the form of parallel rolls along the y axis in an infinite slab of thickness 1. In the lateral direction we will restrict ourselves to the fundamental mode neglecting higher harmonics, while in the z direction (across the layer) a multi-mode description will be used where necessary.

$$
\begin{aligned}
C\,(x,z,t) &= c_0(z,t) + c_1(z,t)\cos kx, && (3.51)\\
\theta(x,z,t) &= \theta_0\,(z,t) + \theta_1\,(z,t)\cos kx, && (3.52)\\
v_x(x,z,t) &= -(1/k)\nabla_z w_1(z,t)\sin kx, && (3.53)\\
v_z(x,z,t) &= w_1(z,t)\cos kx, && (3.54)\\
\phi\,(x,z,t) &= \phi_0\,(z,t) + \phi_1\,(z,t)\cos kx. && (3.55)
\end{aligned}
$$

with incompressibility already built in. We can get rid of the external potential ϕ_e by solving equation (3.44) explicitly. The solutions that vanish at $z = \pm\infty$ and fulfill the boundary condition (3.50) are $\phi_e = \exp(\frac{k}{2})\exp(\mp kz)\phi_1(z{=}\pm\frac{1}{2},t)\cos kx$ for the range $\{1/2,\infty\}$ and $\{-1/2,-\infty\}$, respectively. The boundary conditions (3.49) can then be written in final form

$$
\begin{aligned}
\bar{\epsilon}(\nabla_z\phi_1 + \psi_m c_1) \pm k\phi_1\,|_{z=\pm\frac{1}{2}} &= 0 && (3.56)\\
\nabla_z\phi_0 + \psi_m c_0\,|_{z=\pm\frac{1}{2}} &= 0 && (3.57)
\end{aligned}
$$

Substituting Eqs. (3.51)-(3.55) into the nonlinear equations of motion (3.39)-(3.43) and

sorting for different lateral dependencies yields the following system of equations

$$\begin{aligned}
\frac{1}{Pr}\partial_t\left(\nabla_z^2-k^2\right)w_1 &= -Ra\,k^2\,[(1+M_1)\theta_1-(\psi+M_1\psi_m)c_1-M_1\nabla_z\phi_1]+(\nabla_z^2-k^2)^2w_1 \\
&\quad +Ra\,M_1k^2\left(\theta_1-\psi_m c_1-\nabla_z\phi_1\right)\nabla_z\left(\theta_0-\psi_m\,c_0\right), && (3.58)\\
\partial_t c_0+\tfrac{1}{2}\nabla_z\left(w_1c_1\right) &= L\nabla_z^2\left[(1+M_2\psi_m)c_0+(1-M_2)\theta_0\right], && (3.59)\\
\partial_t c_1+w_1\nabla_z c_0 &= L\left(\nabla_z^2-k^2\right)\left(c_1+\theta_1-M_2\nabla_z\,\phi_1\right), && (3.60)\\
\partial_t\,\theta_0+\tfrac{1}{2}\nabla_z\left(w_1\theta_1\right) &= \nabla_z^2\,\theta_0, && (3.61)\\
\partial_t\,\theta_1+w_1\nabla_z\,\theta_0 &= -w_1+\left(\nabla_z^2-k^2\right)\theta_1, && (3.62)\\
\left(\nabla_z^2-M_3k^2\right)\phi_1 &= \nabla_z\left(\theta_1-\psi_m c_1\right), && (3.63)
\end{aligned}$$

The field ϕ_0 has already been eliminated with the help of $\nabla_z^2\phi_0=\nabla_z(\theta_0-\psi_m c_0)$. This has also been used to write the remaining boundary conditions as

$$\begin{aligned}
\nabla_z(c_1+\theta_1-M_2\nabla_z\phi_1)\,|_{z=\pm1/2} &= 0, && (3.64)\\
\nabla_z((1+M_2\psi_m)c_0+(1-M_2)\theta_0)\,|_{z=\pm1/2} &= 1-M_2, && (3.65)\\
\theta_1\,|_{z=\pm1/2}=\theta_0\,|_{z=\pm1/2} &= 0, && (3.66)\\
w_1\,|_{z=\pm1/2}=\nabla_z w_1\,|_{z=\pm1/2} &= 0, && (3.67)
\end{aligned}$$

To solve this boundary-value problem we adopt vertical profiles w_1, θ_0, θ_1, c_0, c_1 and ϕ_1 in the form

$$\begin{aligned}
w_1(z,t) &= A(t)\cos^2(\pi z), && (3.68)\\
\theta_1(z,t) &= B(t)\cos\pi z, && (3.69)\\
\theta_0(z,t) &= G(t)\sin 2\pi z, && (3.70)\\
c_0(z,t) &= \frac{1-M_2}{1+\psi_m M_2}(z-\theta_0(z,t))+\sum_{n=0}^{n=N}a_n(t)\sin(2n+1)\,\pi z, && (3.71)\\
c_1(z,t) &= -\theta_1(z,t)+\sum_{n=0}^{n=N}b_n(t)\cos 2n\pi z, && (3.72)\\
\phi_1(z,t) &= A_0(t)\,z+\sum_{n=0}^{n=N_1}\frac{A_n(t)\sin 2\pi n z}{2\pi n} && (3.73)
\end{aligned}$$

which satisfy the boundary conditions (3.56,3.64-3.67) identically, if $A_0(2+k)+\sum_{n=1}^{N_1}(-)^nA_n+\psi_m\sum_{n=1}^{N}(-)^nb_n=0$ is chosen.

We point out that for $\psi=0$, and $\psi_m=0$ the concentration fields decouple from temperature and velocity. This reduces Eqs. (3.68)-(3.70) in the absence of the magnetic field to the 3-mode model introduced by Lorenz [76] to mimic the dynamics of convective rolls in single-component Rayleigh-Bénard convection. In the case of finite magnetic field this is a somewhat modified Lorenz model for a magnetic fluid [83]. At nonzero ψ and ψ_m, convection is modified by the concentration field but we can adopt the above few-mode expansion for temperature and velocity [9] without modifications, because the diffusivities for heat and momentum are large enough to prevent the appearance of strong gradients. By way of contrast, owing to the small

Lewis number, the concentration field does build up steep boundary layers, which we account for by a N-mode Fourier series as given in (3.71,3.72). The situation with a magnetic field is somewhat intermediate, since the magnetic potential is coupled dynamically (3.63) and by the boundary conditions (3.56) to the concentration field with its strong gradients. We use a multimode expansion for the magnetic field with a number of modes N_1 which is selected independently of N. For c_0 the modes are antisymmetric in z, while for c_1 symmetric modes are appropriate. The numbers N and N_1 of the contributing modes was taken large enough to ensure that the results are insensitive against a further increase of these numbers. For the parameter values considered here, $N = 50$ and $N_1 = 50$ turned out to be sufficient.

3.6 Approximate analytical solution

In this section we derive an approximate analytical stationary solution, which fits the numerical solution, described above, very well. To get this solution, we make use of the fact that $L \sim 10^{-4}$ is extremely small. Starting with the system of equations (3.58)-(3.63), we use the Lorenz representation of the temperature and velocity field (3.68)-(3.70) and derive approximate solutions for c_0, c_1 and ϕ_1 avoiding the complicated mode expansion (3.71)-(3.73).

Let us first consider equation (3.59). In the stationary case, we can integrate this equation once. With the boundary conditions (3.65) and (3.67) we find

$$\tfrac{1}{2}\,(w_1 c_1) = L\nabla_z\,[(1 + M_2\psi_m)c_0 + (1 - M_2)\theta_0] - L(1 - M_2). \tag{3.74}$$

Far from the boundaries c_0 and c_1 are $\sim L$. This can easily be seen from the consistency of Eq. (3.61) with Eq. (3.74) taking into account that far from the boundaries the derivatives of the functions are small. Thus, in Eq. (3.74) we can neglect c_0, when we are far from the boundaries. Futhermore, we can neglect $\nabla_z\theta_0$ compared to 1, since its influence is very weak [72]. This latter approximation is good, when the amplitude of the velocity is still small, since θ_0 is the nonlinear term in the Lorenz model. Taking this into account we can get the concentration field far from the boundaries as

$$c_1 = -2L(1 - M_2)/w_1. \tag{3.75}$$

To satisfy the boundary conditions for c_1 and to find the profile of the concentration field near the boundaries one needs to solve the boundary layer problem. The expression (3.75) diverges close to the boundaries as $1/(z-1/2)^2$ (if the boundary is on $z = 1/2$). Thus, the solution of the boundary layer problem has to behave asymptotically like $1/(z - 1/2)^2$ far from the boundary, in order to match with Eq. (3.75). The boundary layer problem for the concentration field is considered in App. 3.9.1

Since the boundary-layer depth δ is proportional $L^{1/3}$ (cf. App. 3.9.1) the contribution of the boundary layers gives only small $\sim L^{1/3}$ corrections to the amplitude equation and the expression (3.75) can be used with $w_1 = A\cos^2(\pi z)$.

The next step is to calculate the magnetic field potential ϕ_1 from Eq. (3.63). To do that we split the magnetic potential into two parts, $\phi_1 = \phi_{11} + \phi_{12}$ so that

$$\left(\nabla_z^2 - M_3 k^2\right)\phi_{11} = \nabla_z\,\theta_1, \tag{3.76}$$

$$\left(\nabla_z^2 - M_3 k^2\right)\phi_{12} = -\psi_m \nabla_z\,c_1. \tag{3.77}$$

$$\tag{3.78}$$

with the boundary conditions

$$\bar{\epsilon}\nabla_z\phi_{11} \pm k\phi_{11}\,|_{z=\pm\frac{1}{2}} = 0 \tag{3.79}$$

$$\bar{\epsilon}(\nabla_z\phi_{12} + \psi_m c_1) \pm k\phi_{12}\,|_{z=\pm\frac{1}{2}} = 0 \tag{3.80}$$

The solution for ϕ_{11} is straightforward and simple when we take the temperature field in the form of Eq. (3.69)

$$\phi_{11} = \frac{\pi B}{\pi^2 + a^2}\left(\sin(\pi z) - \frac{k\sinh(az)}{k\sinh(\frac{a}{2}) + \bar{\epsilon}a\cosh(\frac{a}{2})}\right) \tag{3.81}$$

with $a = \sqrt{M_3}k$. The solution for ϕ_{12} has the form

$$\phi_{12} = M\sinh(az) - \frac{\psi_m}{a}\left(\sinh(az)\int_0^z \cosh(a\xi)c_1'(\xi)d\xi - \cosh(az)\int_0^z \sinh(a\xi)c_1'(\xi)d\xi\right) \tag{3.82}$$

with M a constant of integration. Note that $\phi_{12}(z)$ has to be an antisymmetric function in z. To find M we consider the boundary condition (3.80). This is done in App. 3.9.2 with the final result

$$\phi_{12}(z) = \alpha(1 - M_2)\left(\frac{L^2}{\pi^4 A^2(1 + \psi_m M_2)}\right)^{1/3}\frac{k\psi_m}{k\sinh(\frac{a}{2}) + \bar{\epsilon}a\cosh(\frac{a}{2})}\sinh(az) + O(L), \tag{3.83}$$

where $\alpha = -\int_0^\infty \zeta f'(\zeta)d\zeta \approx 2.791$ is a real number of order 1 independent of any parameter of the problem, and the function $f(\zeta)$ is defined in Eq. (3.97) in App. 3.9.1.

Having found an approximate expression for the profiles of the concentration and magnetic potential we substitute them into Eq. (3.59) and then project this equation on the weight function $\cos^2(\pi z)$. Equations (3.62) and (3.63) are to be projected with the weight functions $\sin(2\pi z)$ and $\cos(\pi z)$, respectively. This leads to a system of three algebraic equations for the amplitudes A, B, G (3.68)-(3.70), from which we get the final (implicit) expression for the saturation amplitude A as a function of the parameters of the problem

$$\begin{aligned}\frac{18\pi^4}{Ra} &= \frac{1 + M_1(\beta - 2\pi\bar{\beta}G)}{1 + \frac{3}{40\pi^2}A^2} \\ &\quad + (1 - M_2)\frac{32\pi^2}{3A^2}\left[L(\psi + M_1\psi_m) + \gamma(1 - \bar{\gamma}G)M_1\psi_m\left(\frac{L^2 A}{1 + \psi_m M_2}\right)^{1/3}\right]\end{aligned} \tag{3.84}$$

Here

$$\beta = 1 - \frac{\pi^2}{\pi^2 + a^2} + \frac{3\pi^5\sinh(\frac{a}{2})}{(\pi^2 + a^2)(4\pi^2 + a^2)(\pi\sinh(\frac{a}{2}) + \bar{\epsilon}a\cosh(\frac{a}{2}))}, \tag{3.85}$$

$$\bar{\beta} = \frac{3}{5}(1 - \frac{\pi^2}{\pi^2 + a^2}) + \frac{\pi^2}{\pi^2 + a^2}\frac{a}{(\pi\sinh(\frac{a}{2}) + \bar{\epsilon}a\cosh(\frac{a}{2}))}\frac{3\pi^3(8\pi^2 - a^2)\sinh(\frac{a}{2})}{a(a^4 + 20a^2\pi^2 + 64\pi^4)}, \tag{3.86}$$

$$\gamma = \alpha\frac{2\pi^{5/3}\sinh(\frac{a}{2})}{(a^2 + 4\pi^2)(\pi\sinh(\frac{a}{2}) + \bar{\epsilon}a\cosh(\frac{a}{2}))}, \tag{3.87}$$

$$\bar{\gamma} = \pi - \frac{3\pi a^2}{a^2 + 16\pi^2}, \tag{3.88}$$

G, the stationary amplitude of θ_0 Eq. (3.70), is

$$G = \frac{9A^2}{160\pi^3(1+\frac{3}{40\pi^2}A^2)}, \tag{3.89}$$

while $B = (5\pi^2/2A)G$. In the Eq. (3.84) we have chosen $k = \pi$ in order to simplify the formula. This is reasonable, since the wave number of the maximum growth k_c is close to π. The second line of Eq. (3.84) can be seen as an expansion in $\psi_m L^{2/3}$ and ψL. Since the prefactor of the former is pretty small, we have also kept the leading contribution to the order $\psi_m L$. The complete evaluation of the $\psi_m L$ term is hardly worth doing, since it makes formula (3.84) unnecessary complicated without significantly changing the quantitative results. The occurrence of fractional powers of A and L as products with ψ_m and M_1 indicates the importance of the boundary layers in the case of an external field.

3.7 Influence of the Kelvin force

We first investigate the influence of the Kelvin force on the convection and disregard magnetophoresis for the moment by putting $M_2 = 0$. The equations for the mode amplitudes A, B, G, a_n, b_n have been solved by a Runge-Kutta integration. The wave number k, usually taken to characterize the mode of maximum linear growth rate $\lambda(k, Ra)$, varies between 3 and 3.5 within the investigated Rayleigh number regime. However, since the final predictions of our model turn out not to depend sensitively on the k-value chosen, we adopt in all of our simulations $k = 3.1$. All runs are started form the initial configuration of an undisturbed linear temperature and magnetic field profile and a constant concentration as given in Eqs. (3.36) - (3.38), and small random velocity fluctuations to start the convection process.

In all of our runs the convective motion was found to settle in a stationary convection the same way as it is in the absence of magnetic field [9]. There are roughly three different regimes of the time evolution: linear growth, nonlinear transition to a saturation state, and the saturation state itself. When we fix the temperature gradient (i.e. take the Rayleigh number constant) and change the magnetic field strength, we have the bifurcation picture as a function of M_1. This is the most convenient bifurcation curve to compare with experiment, since during experiments it is much easier to change M_1 (i.e. the magnetic field) than the Rayleigh number (i.e. the temperature difference). This bifurcation diagram is shown in Fig. 4.1 for different values of the separation ratios ψ and ψ_m. These two parameters are related to the two different mechanisms of how the concentration inhomogeneity changes the bifurcation picture. The separation ratio ψ is independent of the magnetic nature of the grains and describes the concentration buoyancy force due to the density difference of the solvent liquid and the magnetic grains. The second mechanism is due to the Kelvin force that arise from the concentration variations of the magnetic particles and the resulting strong variations of the magnetic susceptibility. This effect relies on the magnetic nature of the ferrofluid particles and is characterized by the magnetic separation ratio ψ_m.

Without any concentration variations ($\psi_m = 0$, and $\psi = 0$) we have the usual pitchfork bifurcation with respect to M_1 (Fig. 3.1). If only the non magnetic mechanism is switched on ($\psi = 10$, $\psi_m = 0$), the bifurcation looks like an imperfect one with a non zero saturation amplitude even in the subcritical parameter range. In the supercritical parameter range

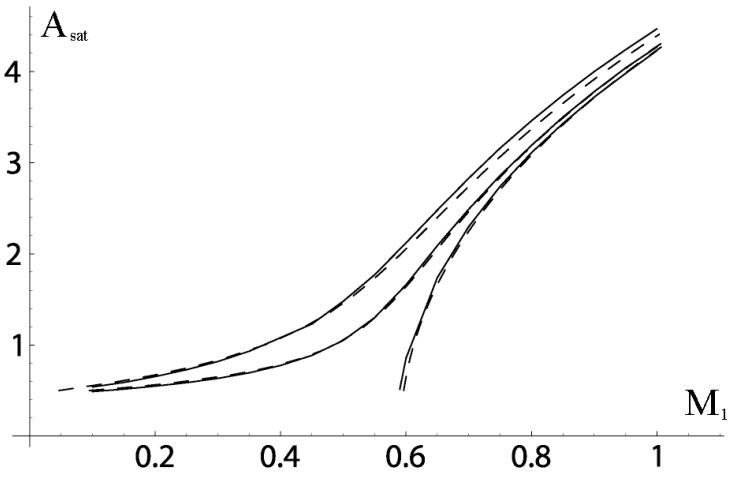

Figure 3.1: The saturation amplitude $A_{sat} = A(t \to \infty)$ as a function of M_1 at $Ra = 1300$ for different values of ψ and ψ_m (see text). The dashed lines are the analytical result (3.84).

the amplitude approaches that of the homogenous ferrofluid. If we switch on additionally the magnetic buoyancy effect ($\psi_m = 10$), the bifurcation deviates strongly from the previous cases and, in particular, has a different saturation behavior for strong magnetic fields. We should point out that in order to get this numerical result at least 50 modes, each for the concentration and magnetic field, have to be taken into account. Comparing this to the case without a magnetic field [9], when 20 modes were more than enough, we can see the importance of the boundary layers when the magnetic field is on. In Fig. 3.1 the analytical results, Eq. (3.84), are shown as dashed lines. The agreement between the numerical and analytical result is very good.

Influence of magnetophoresis

In this section we discuss the influence of magnetophoresis ($M_2 \neq 0$). In the implicit equation for the amplitude, Eq. (3.84), the magnetophoretic effect is manifest in two different ways. First, there is the global pre-factor $(1 - M_2)$ in the second line and, second, there is the denominator $(1 + M_2\psi_m)^{1/3}$ in the term proportional to $L^{2/3}$. Since M_2 is negative (but $M_2\psi_m > -1$, cf. the discussion after Eq. (3.44)), both effects grow with the external field.

The second effect gets very pronounced, when the product $M_2\psi_m$ approaches its stability limit -1. This happens for a magnetic field $H_0 \to H_c$ with $H_c^2 = \gamma_H \bar{\epsilon}\, \chi_c^{-2}$, where, however, the susceptibilities may themselves be (weak) functions of H_0^2 for strong fields. In that limit the boundary layer becomes singular, which is indicated in the numerical approach by the necessity to take into account more and more spatial modes. The analytical treatment also breaks down and Eq. (3.84) is no longer a good description. The breakdown of thermodynamic stability also shows up in the diffusion equation for the concentration

$$\partial_t c(z,t) = L(1 + \psi_m M_2)\nabla_z^2 c(z,t) \tag{3.90}$$

that follows from Eqs. (3.41) and (3.43) under the assumption that the temperature equilibrates much faster. For $H_0 \to H_c$ the diffusional time scale diverges and, therefore, the boundary layer profile gets sharper. This can also be inferred from the Eq. (3.98), which shows the boundary

layer depth to scale with $(L(1+\psi_m M_2))^{1/3}$. For the amplitude the effect of M_2 is very weak and hardly visible in a plot like Fig. 4.1, except for the immediate vicinity of the stability limit $(1+M_2\psi_m)=0$.

The breakdown of thermodynamic stability may be related to particle agglomeration and internal structure formation. The magnetophoretic effect is due to the force, which drives magnetic particles to areas of larger magnetic field strength. This leads to agglomerations, where the magnetic field is larger and consequently attracts further particles. This mechanism is compensated by the (magnetic-field independent) diffusive motion or the particles. When the strength of the magnetic field exceeds a certain value, the diffusion fails to prevent agglomeration of the particles and structures are built. In that case the description in terms of an ordinary binary mixture is no longer possible.

3.8 Conclusion (Chap. 3)

We have derived the complete set of equations to describe ferrofluids in an external magnetic field in terms of a binary mixture. Magnetophoretic effects as well as magnetic stresses have been taken into account in the static and dynamic part of the equations. They were used to investigate the thermal convection instability of ferrofluids in the presence of an external magnetic field. As in the case without a magnetic field, the effect of the concentration field is manifest in an apparent imperfection of the bifurcation. A magnetic field makes this imperfection more pronounced. More important however, an external magnetic field not only leads to pronounced boundary layer profiles (with respect to concentration and magnetic potential), this boundary layer also couples effectively to the bulk behavior due to the magnetic boundary condition. This makes the numerical solution of the bifurcation problem considerably more complicated than without a magnetic field. Nevertheless, we were able to present an approximative analytical solution by taking into account part of the boundary layer behavior, explicitly. The agreement between the analytical and the numerical solution was very good. We also discuss the limitations of the binary mixture model. In a strong external field diffusion fails to prevent agglomeration of the particles due to magnetophoresis. In that case the breakdown of the binary mixture model shows up by the occurrence of a negative effective diffusion constant.

3.9 Appendix (Chap. 3)

3.9.1 The boundary layer problem

We consider Eqs. (3.60), (3.74), and (3.80) in the vicinity of the boundary $z=1/2$. Near the boundary the derivatives with respect to z of the functions c_0, c_1 and ϕ are large and we use this fact to simplify these three equations as

$$\frac{1}{2}(w_1 c_1) = L(1+M_2\psi_m)c_0' - L(1-M_2), \tag{3.91}$$

$$w_1 c_0' = L\,(c_1'' - M_2\,\phi_{12}'''), \tag{3.92}$$

$$\phi_{12}'' = -\psi_m c_1', \tag{3.93}$$

under the assumptions

$$\phi_{11}''' \ll \phi_{12}''' \quad \text{and} \quad \nabla_z^2 \gg \mathrm{k}^2, \tag{3.94}$$

Combining these three equations into one we get an equation for c_1

$$\frac{1}{2} w c_1 = \frac{L^2(1+M_2\psi_m)^2}{w} c_1'' - L(1-M_2). \tag{3.95}$$

Near the boundary $z = -1/2$ we have $\varepsilon = z - 1/2 \ll 1$. Expanding $\cos^2(\pi z)$ in powers of ε the velocity $w_1 = A\pi^2\varepsilon^2$ and Eq. (3.95) takes the form

$$\frac{\pi^2 A}{2L(1-M_2)} \varepsilon^4 c_1 = \frac{L(1+M_2\psi_m)^2}{\pi^2 A(1-M_2)} c_1'' - \varepsilon^2. \tag{3.96}$$

We rescale the concentration field and z coordinate in such a way that the final equation becomes independent of any parameters and appears to be a universal equation defining the boundary layer profile

$$\frac{1}{2}\zeta^4 f + \zeta^2 = f'', \tag{3.97}$$

with

$$\zeta = \left(\frac{\pi^2 A}{L(1+\psi_m M_2)}\right)^{1/3} \varepsilon, \qquad c_1(z) = (1-M_2)\left(\frac{L}{\pi^2 A(1+\psi_m M_2)^2}\right)^{1/3} f(\zeta). \tag{3.98}$$

Thus, the layer depth δ scales with $L^{1/3}$. We assume that the boundary condition (3.64) for the concentration field c_1 can be replaced by a homogeneous one $c_1'(\pm 1/2) = 0$ leading to $f'(0) = 0$. In this case the boundary layer profile becomes self-similar. As a second boundary condition we require that the function $f(\zeta)$ has the asymptotic form $f(\zeta) \to -2/\zeta^2$ when $\zeta \to \infty$, in order to be compatible with the bulk solution (3.75). In Fig. 3.2 we compare the boundary layer profiles that follow from the analytical solution (3.97)-(3.98) with those obtained numerically. The approximation $f'(0) = 0$ is good, when M_1 is not too large, e.g. for $M_1 = 0.1$ the agreement between numerics and analytics is better than for $M_1 = 1.0$. The important quantity we extract from the boundary layer considerations and that enters Eq. (3.84) is $\alpha = \int_0^\infty \xi f'(\xi) d\xi$. The error made by calculating this number using the condition $f'(0) = 0$ is of the order of 30% when compared with the numerical result for $M_1 = 1.0$, where $f'(0) \approx -0.5$ (Fig. 3.2). This correction would change the analytically determined amplitudes, Eq. (3.84), shown in Fig. 3.1 as dashed lines only by about 1%.

3.9.2 Calculation of the magnetic field ϕ_{12}

To fulfill the boundary conditions for the magnetic potential we need to plug the expression (3.82) into Eq. (3.80). Doing so we get the integrals of the type

$$\int_0^{1/2} \cosh(a\xi) c_1'(\xi) d\xi, \quad \int_0^{1/2} \sinh(a\xi) c_1'(\xi) d\xi \tag{3.99}$$

which would diverge, if we would simply use expression (3.75) for the concentration field. To resolve these singularities we have solved the boundary layer problem for the concentration

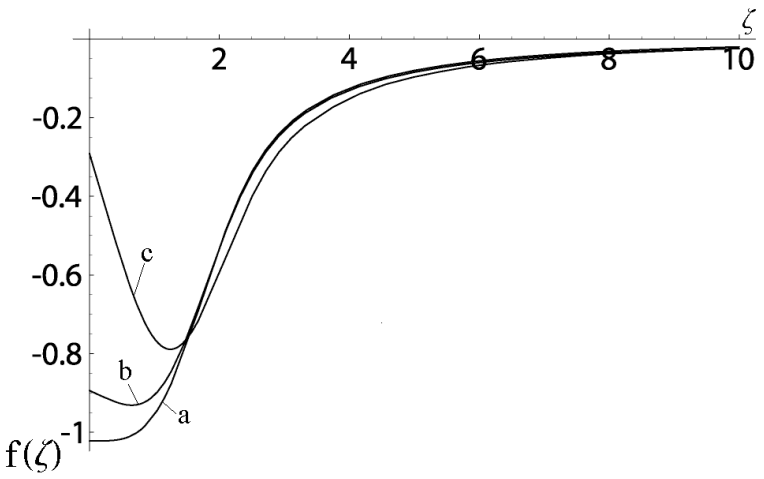

Figure 3.2: The boundary layer profiles obtained from a) the analytical solution $f(\zeta)$, Eq. (3.97), b) the multi-mode numerical solution scaled with (3.98) for $M_1 = 0.1$, and c) for $M_1 = 1.0$ ($M_2 = 0$, $\psi = 10$ and $\psi_m = 10$).

field in the preceding section. Let us consider the first integral, the second one is treated in the same way. We can divide this integral into two parts

$$\int_0^{1/2} \cosh(a\xi) c_1'(\xi) d\xi = \int_0^{1/2-\Delta} \cosh(a\xi) c_1'(\xi) d\xi + \int_{1/2-\Delta}^{1/2} \cosh(a\xi) c_1'(\xi) d\xi. \tag{3.100}$$

Here Δ is a small, but fixed value, chosen in such a way that for $z > \Delta$ the bulk profile (3.75) and and for $z < \Delta$ the boundary layer profile (3.98) are valid. In the second integral we can expand $cosh(a\xi)$ in the vicinity of $\xi = 1/2$. Then we can write

$$\begin{aligned} \int_{1/2-\Delta}^{z} \cosh(a\xi) c_1'(\xi) d\xi &= \cosh(\frac{a}{2}) \int_{1/2-\Delta}^{z} c_1'(\xi) d\xi + a \sinh(\frac{a}{2}) \int_{1/2-\Delta}^{z} (\xi - 1/2) c_1'(\xi) d\xi + \ldots \\ &\equiv \cosh(\frac{a}{2}) I_0(z) + a \sinh(\frac{a}{2}) I_1(z) + \frac{a^2}{2} \cosh(\frac{a}{2}) I_2(z) + \ldots \end{aligned} \tag{3.101}$$

for $z \to 1/2$. Since c_1' is regular at the boundary and the boundary layer depth $\delta \sim L^{1/3}$, the expansion (3.101) is actually an expansion in powers of $L^{1/3}$.

If we substitute the expression (3.101) [and the appropriate one for the second integral in Eq. (3.99)] into the potential ϕ_{12} (3.82), the boundary condition (3.80) for $z = 1/2$ takes the form

$$M \left(k \sinh(\frac{a}{2}) + \bar{\epsilon} a \cosh(\frac{a}{2}) \right) + k\psi_m I_1(z \to 1/2) + \bar{\epsilon} \left[-I_0(z \to 1/2) + c(1/2) \right] + \ldots = 0 \tag{3.102}$$

where the dots indicate terms of O(L), e.g., $I_2(z \to 1/2)$. From the definition of $I_0(z)$ we can see that the leading contributions in the brackets cancel and only terms $\sim L^{2/3}$ are left. Thus, the main contribution to M is proportional to the integral $I_1(z \to 1/2)$

$$M = -\frac{k\psi_m}{k \sinh(\frac{a}{2}) + \bar{\epsilon} a \cosh(\frac{a}{2})} I_1(z \to 1/2) \tag{3.103}$$

With the expression (3.98) we can calculate the integral $I_1(z \to 1/2)$

$$\begin{aligned} I_1(z \to 1/2) &= \int_{1/2-\Delta}^{1/2} (\xi - 1/2) c_1'(\xi) d\xi \\ &= -(1 - M_2) \left(\frac{L^2}{\pi^4 A^2 (1 + \psi_m M_2)} \right)^{1/3} \int_0^\infty \zeta f'(\zeta) d\zeta + O(L) \end{aligned} \quad (3.104)$$

where we have replaced Δ as the upper limit of the integral by ∞. The error introduced is canceled by the first integral of Eq. (3.100), (which we have not considered so far) if the bulk and boundary-layer concentration fields c_1 are matched at $z = \Delta$. Since in the bulk $c_1 \sim L$, the remaining contribution of the first integral in Eq. (3.100) is of $\mathrm{O}(L)$, which we neglect. Finally, the magnetic field ϕ_{12} in the bulk of the layer takes the form

$$\phi_{12}(z) = \alpha (1 - M_2) \left(\frac{L^2}{\pi^4 A^2 (1 + \psi_m M_2)} \right)^{1/3} \frac{k \psi_m}{k \sinh(\frac{a}{2}) + \bar{\epsilon} a \cosh(\frac{a}{2})} \sinh(az) + O(L), \quad (3.105)$$

where $\alpha = \int_0^\infty \zeta f'(\zeta) d\zeta \approx 2.791$ is a real number independent of any parameter of the problem.

Chapter 4

Hydrodynamic instabilities in ferronematics

4.1 Introduction

In the last 20 years the study of nonlinear nonequilibrium phenomena in spatially extended systems, with particular emphasis on pattern-forming phenomena, has been one of the very active areas in physics, exhibiting interesting ramifications into other sciences. During this time the study of the "classic" systems, like Rayleigh-Bénard convection and Saffman-Taylor instability in simple fluids, has also been supplemented by the study of more complex systems. Here liquid crystals have played and are still playing, a major role. They are full of nonlinearities and give rise to new symmetry classes, which are sometimes actually simpler to deal with qualitatively, but they still allow a quantitative description of experiments in many cases. In fact, one of the attractions of the field is the close contact between experiment and theory. A good introduction to the recent development of the field of instabilities and pattern-formation in liquid crystals can be found in [84].

When we deal with ferronematic liquid crystals, rather than simple nematics, the theoretical description becomes more complicated. This is due to the fact that ferronematics are more sensitive to magnetic fields, and those magnetic field effects, which can be safely neglected in conventional nematics, may become important in ferronematics [57].

In this chapter we address the question, what are the consequences of the new linear magnetic field effects derived in [57] on hydrodynamic instabilities in ferronematics. In particular, we consider the well-known Rayleigh-Bénard and Saffman-Taylor instabilities and discuss how the general features of these instabilities are changed qualitatively due to the presence of the new contributions [79]. The qualitatively new behavior can be used as a tool to measure the new field-dependent material parameters involved [57].

We disregard the magnetization as an independent dynamic degree of freedom, but assume that it is relaxed to its equilibrium value and orientation on the time scale under consideration. This is in the spirit of the "rigid anchoring" approximation [37], implying that the relative orientation of the director $\mathbf{n}$ and the local magnetization $\mathbf{M}$ is fixed (being either parallel or perpendicular). However, with the synthesis of thermotropic ferronematics [85] it became evident that this approximation might not be generally applicable. The orientations of $\mathbf{n}$ and $\mathbf{M}$ were treated as separate degrees of freedom within the framework of a microscopic

model [86] and in a hydrodynamic description [59]. We also assume that there is no spontaneous magnetization (true ferromagnetism), that means there is no remnant magnetization in the absence of an external field. Although such a ferromagnetic behavior is possible in principle [87], there is yet no experimental evidence for it.

The chapter is organized as follows. In the next section we recap the governing equations and simplify them for particular cases of interest. In section 4.3 we address the problem of the Rayleigh-Bénard convection in ferronematics for two different cases - positive and negative magnetic susceptibility anisotropy. Section 4.4 presents a linear analysis of viscous fingering in a radial Hele-Shaw cell for ferronematics.

4.2 Governing equations

As discussed in the preceding section we take the set of hydrodynamic equations given in [57] to describe ferronematics. Since we will use them to discuss Rayleigh-Bénard and Saffman-Taylor instabilities, we will apply the well-known Boussinesq approximation [74], i.e. take the flow as incompressible and all material parameters as well as the density as constant (ρ_0), except for the buoyancy force. We are then left with dynamic equations for the velocity field $\boldsymbol{v}$, the temperature T, and the director field $\boldsymbol{n}$

$$\rho(\frac{\partial v_i}{\partial t} + v_j\nabla_j v_i) = -\nabla_i p + \nu_{ijkl}\nabla_j\nabla_k v_l + \frac{1}{2}\tilde{\lambda}_{kji}\nabla_j h_k - \nabla_j(\Phi_{li}\nabla_i n_l) + \rho g_i \tag{4.1}$$

$$\mathrm{div}\boldsymbol{v} = 0 \tag{4.2}$$

$$\frac{C_V}{T}(\frac{\partial T}{\partial t} + v_i\nabla_i T) = \kappa_{ij}\nabla_i\nabla_j T \tag{4.3}$$

$$\frac{\partial n_i}{\partial t} + v_j\nabla_j n_i = -\frac{1}{2}\lambda_{ijk}\nabla_j v_k + (\gamma^{-1})_{ij}h_j \tag{4.4}$$

where on the r.h.s. of (4.3) dissipative nonlinearities (e.g. "viscous heating") have been neglected. C_V is the specific heat at constant density, p is the pressure, $\boldsymbol{g}$ is the constant gravity force, while $\boldsymbol{h} \equiv \partial\epsilon/\partial\boldsymbol{n}$ (with ϵ the energy density) and $\Phi_{ij} \equiv \partial\epsilon/\partial\nabla_j n_i$ are the thermodynamic conjugates to homogeneous and inhomogeneous director reorientations [78]. The former describes the static response to external fields, while the latter contains the Frank rotational elasticity. The induced magnetization is assumed to be fixed by the external field and is not a dynamic variable. The concentration of magnetic particles is very low and we neglect the Kelvin force.

The material tensors, in linear order of the external magnetic field, are the sum of a constant part and a linear one

$$\nu_{ijkl} = \nu^D_{ijkl} + \nu^R_{ijkl}(H) \tag{4.5}$$

$$\kappa_{ij} = \kappa^D_{ij} + \kappa^R_{ij}(H) \tag{4.6}$$

$$\lambda_{ijk} = \lambda^R_{ijk} + \lambda^D_{ijk}(H) \tag{4.7}$$

$$\tilde{\lambda}_{kji} = \lambda^R_{kji} - \lambda^D_{kji}(H) \tag{4.8}$$

$$(\gamma^{-1})_{ij} = (\gamma^{-1})^D_{ij} + (\gamma^{-1})^R_{ij}(H) \tag{4.9}$$

and describe viscosity [88], heat conduction, flow alignment and director relaxation, respectively. Their general form is listed in [57, 78] and will be given below, as far as needed. Note that

the thermodynamic nature of the different contributions changes from dissipative (superscript D) to reversible (superscript R), or vice versa, since the magnetic field transforms odd under time reversal. Thus, the field-free contributions to the dynamics always have a different time reversal behavior compared to those linear in the field, which in turn gives rise to the different thermodynamic properties. This is reflected also in the different symmetry properties (Onsager relations), i.e. symmetric in the dissipative parts ($\kappa^D_{ij} = \kappa^D_{ji}$, $\nu^D_{ijkl} = \nu^D_{klij}$, $(\gamma^{-1})^D_{ij} = (\gamma^{-1})^D_{ji}$) and antisymmetric in the reversible parts ($\kappa^R_{ij}(H) = -\kappa^R_{ji}(H)$, $\nu^R_{ijkl}(H) = -\nu^R_{klij}(H)$, $(\gamma^{-1})^R_{ij}(H) = -(\gamma^{-1})^R_{ji}(H)$) and in the difference between λ_{ijk} and $\tilde{\lambda}_{ijk}$ in (4.1) and (4.4).

It is the purpose of this work to investigate the influence of the linear field contributions to the transport tensors (and mainly that of $\nu^R_{ijkl}(H)$) on various instabilities. We do this in the approximation of very strong fields, since in that limit there is the best chance that the proposed new effects are observable. Specifically we assume that the director relaxes to its equilibrium orientation, defined by the external field, on a time scale much smaller than that of the other relevant variables. In that case $\partial n_i/\partial t = 0$ and the director is clamped. The larger the field the better is this approximation. For ordinary nematics (5CB) the field necessary to clamp the director is about 1 kGauss [89] and probably smaller for ferronematics, since their response to magnetic fields generally is stronger.

This approximation is similar in spirit to the incompressibility assumption, where the density variations are supposed to live on a much shorter time scale than the other relevant variables (i.e. the relevant velocities are much smaller than the sound velocity). When density variations are not a dynamic variable, its conjugate, the chemical potential or the pressure is no longer determined thermodynamically. The pressure is used to guarantee the incompressibility for all times, i.e. $\partial \mathrm{div}\boldsymbol{v}/\partial t = 0$, which leads to a condition on $\boldsymbol{\nabla}^2 p$ in Eq. (4.1). Eliminating the director as a dynamic variable has the consequence that its conjugate, $\boldsymbol{h}$ is not defined, but rather functions to guarantee $\boldsymbol{n} = const.$ for all times, thus reducing Eq. (4.4) to

$$h_i = \gamma_{ji}\frac{1}{2}\lambda_{jkl}\nabla_k v_l \tag{4.10}$$

where $\gamma_{pm}(\gamma^{-1})_{mq} \equiv \delta^{tr}_{pq}$. Substituting this in (4.1) we regain for this equation a form familiar from simple liquids

$$\rho(\frac{\partial v_i}{\partial t} + v_j\nabla_j v_i) = -\nabla_i p + \nu^{eff}_{ijkl}\nabla_j\nabla_k v_l + \rho g_i \tag{4.11}$$

but with an effective viscosity tensor

$$\nu^{eff}_{ijkl} = \nu_{ijkl} + \frac{1}{4}\tilde{\lambda}_{pji}\gamma_{pm}\lambda_{mkl} \tag{4.12}$$

Since we are concentrating on linear field effects Eq. (4.12) can be simplified

$$\begin{aligned}\nu^{eff}_{ijkl} &= \nu^D_{ijkl} + \nu^R_{ijkl}(H) + \frac{1}{4}\lambda^R_{pji}\gamma^D_{pm}\lambda^R_{mkl} + \frac{1}{4}\gamma^D_{pm}\left(\lambda^R_{pji}\lambda^D_{mkl}(H) - \lambda^D_{pji}(H)\lambda^R_{mkl}\right)\\ &\quad + \frac{1}{4}\lambda^R_{pji}\gamma^R_{pm}(H)\lambda^R_{mkl}\end{aligned} \tag{4.13}$$

where the γ_{ij} tensors are given by

$$\gamma^D_{ij} = \gamma_1\delta^{tr}_{ij} \tag{4.14}$$

$$\gamma^R_{ij} = -\frac{\gamma_1^2}{\gamma_1^R}\epsilon_{ijk}n_k n_l H_l - \frac{\gamma_1^2}{\gamma_2^R}\left(\epsilon_{ijp} + \epsilon_{ipk}n_k n_j - \epsilon_{jpk}n_k n_i\right)H_p \tag{4.15}$$

Here the coefficients γ_1^R, γ_2^R are those introduced in [57].

The explicit forms of this effective viscosity tensor will be discussed for the two cases $\boldsymbol{n} \parallel \boldsymbol{H}$ and $\boldsymbol{n} \perp \boldsymbol{H}$ below.

The heat conduction equation (4.3) also contains a new linear field effect through $\kappa_{ij}^R(H)$ (4.6). However, in this case the bulk effect vanishes, since both, $\nabla_i \kappa_{ij}^R = 0$, because of $\boldsymbol{n} = const$ and the Boussinesq approximation, and $\kappa_{ij}^R \nabla_i \nabla_j T = 0$, because of $\kappa_{ij}^R(H) = -\kappa_{ji}^R(H)$. Thus, this linear field effect will only appear in boundary conditions, if they are formulated in terms of the heat flux. We will not consider such boundary conditions in what follows.

In the next section we will investigate how the new terms (4.13) manifest themselves in the thermo-gravitational instability.

4.3 Rayleigh-Bénard instability

4.3.1 The case when $\boldsymbol{n} \parallel \boldsymbol{H}$

We consider an infinitely extended layer of ferronematic liquid crystal bounded by two rigid parallel plates at distance d. The temperature of the plates is kept fixed at T_1 and $T_0 > T_1$ (Fig. 4.1). An external magnetic field is imposed in z-direction ($\hat{\boldsymbol{e}}_z$) and the gravitational force

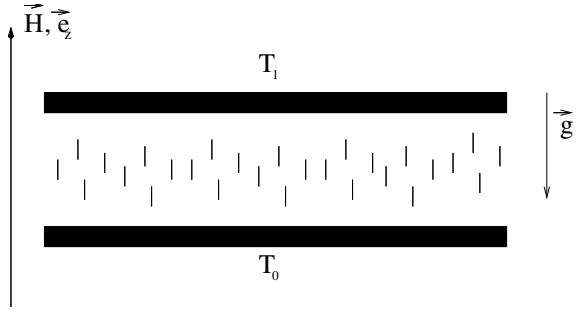

Figure 4.1: Sketch of the setup in the parallel case. For details see text.

works in $-z$-direction ($\boldsymbol{g} = -g\hat{\boldsymbol{e}}_z$). In the case of a positive magnetic susceptibility anisotropy $\chi_a > 0$ the director tends to align along the magnetic field. Homeotropic boundary conditions for the director are helpful. We assume the magnetic field to be strong enough that the director is clamped

$$\boldsymbol{n} = \frac{\boldsymbol{H}}{|\boldsymbol{H}|} \tag{4.16}$$

and does not have an independent dynamics. The magnetic field in the sample is always taken as static and uniform, and equal to the value of external field (eventually corrected by some demagnetization factor). Thus the system is described by the effective Navier-Stokes equation (4.11), incompressibility (4.2) and heat conduction (4.3).

The trivial heat conduction state, without any flow and a linear temperature profile is always

a solution.

$$\begin{aligned} \boldsymbol{v} &= 0 && (4.17)\\ T(z) &= -\frac{T_0 - T_1}{d} z + T_0 && (4.18)\\ \rho(z) &= \rho_0 \left(1 + \alpha_p \frac{T_0 - T_1}{d} z\right) && (4.19) \end{aligned}$$

with $\alpha_p = -(1/\rho)(\partial\rho/\partial T)_p$ the thermal expansion coefficient.

However, this solution is stable for small temperature differences only and is subject to the Rayleigh-Bénard instability, when the temperature difference exceeds some threshold value. To find this threshold value in terms of the material parameters involved, we study the stability of small perturbations of the ground state (4.17-4.19) by linearizing (4.2,4.3,4.11) around the conduction state

$$\begin{aligned} \partial_t v_i &= -\frac{\nabla_i p'}{\rho_0} + \mu^{eff}_{ijkl} \nabla_j \nabla_k v_l - g\,\alpha_p\,\theta \delta_{i,z} && (4.20)\\ \partial_t \theta - w &= k_{ij} \nabla_i \nabla_j \theta && (4.21)\\ div\,\boldsymbol{v} &= 0 && (4.22) \end{aligned}$$

Here $\boldsymbol{v}$ is the velocity field ($w = v_z$), θ is the deviation of the temperature field from the linear profile (4.18) and p' the pressure perturbation. The temperature conduction tensor $k_{ij} = k_\perp (\delta_{ij} - n_i n_j) + k_\parallel n_i n_j$ is related to the heat conduction tensor $\kappa_{ij} = (C_V/T) k_{ij}$ and the effective kinematic viscous tensor $\mu^{eff}_{ijkl} = (1/\rho_0)\nu^{eff}_{ijkl}$ is connected to the effective dynamic viscosity ν^{eff}_{ijkl} (4.12).

The complicated tensors (4.5-4.9) that enter μ^{eff}_{ijkl} can be simplified in the special case $\boldsymbol{n} \parallel \boldsymbol{H}$ considered here with the result

$$\begin{aligned} \rho_0\,\mu^{eff}_{ijkl} &= \nu_2 (\delta_{jl}\delta_{ik} + \delta_{il}\delta_{jk})\\ &\quad +2(\nu_1 + \nu_2 - 2\nu_3 + \tfrac{1}{2}\gamma_1\lambda^2)\, n_i n_j n_k n_l\\ &\quad +(\nu_3 - \nu_2)(n_j n_l \delta_{ik} + n_j n_k \delta_{il} + n_i n_k \delta_{jl} + n_i n_l \delta_{jk})\\ &\quad +\tfrac{1}{4}\gamma_1 \left((\lambda-1)^2 \delta_{jk} n_i n_l + (\lambda+1)^2 \delta_{il} n_j n_k\right)\\ &\quad +\tfrac{1}{4}\gamma_1 (\lambda^2 - 1)(\delta_{jl} n_i n_k + \delta_{ik} n_j n_l)\\ &\quad +H(\bar{\nu}^R_1 \varepsilon_{ikp} n_j n_l n_p + \bar{\nu}^R_2 \varepsilon_{ilp} n_j n_k n_p + \bar{\nu}^R_3 \varepsilon_{jlp} n_i n_k n_p + \bar{\nu}^R_4 \varepsilon_{jkp} n_i n_l n_p)\\ &\quad +\bar{\bar{\nu}}^R H(\varepsilon_{ikp}\delta_{jl} n_p + \varepsilon_{ilp}\delta_{jk} n_p + \varepsilon_{jkp}\delta_{il} n_p + \varepsilon_{jlp}\delta_{ik} n_p) \end{aligned} \quad (4.23)$$

where for the field-free viscosities ($\nu_{1,2,3}$) the Harvard notation [90] is used, λ is the flow alignment parameter [91], and γ_1 the rotational viscosity [92]. The abbreviations $\bar{\nu}^R_\alpha$ and $\bar{\bar{\nu}}^R$ that are related to the new field-dependent effects are listed in App. 4.6.1 (4.41).

We non-dimensionalize equations (4.20-4.22) by taking the layer thickness d as length scale, $d^2/k_\perp$ as time scale and the difference $T_0 - T_1$ as temperature scale. With the usual procedure

[74] of taking $(curl\ curl)_z$ as well as $curl_z$ of the Eq. (4.20) we get for w, $\xi \equiv (curl\boldsymbol{v})_z$ and θ

$$\begin{aligned}
\frac{1}{Pr}\partial_t\left(\Delta_2+\nabla_z^2\right)w &= \left(a\,\nabla_z^4+b\Delta_2\nabla_z^2+c\Delta_2^2\right)w+Ra\,\Delta_2\theta \\
&\quad +\overline{H}_1\left(e\Delta_2-\nabla_z^2\right)\nabla_z\xi-\overline{H}_2\left(\Delta_2+\nabla_z^2\right)\nabla_z\xi \qquad (4.24)\\
\frac{1}{Pr}\partial_t\xi &= \left(\Delta_2+a\,\partial_z^2\right)\xi-\overline{H}_1\left(d\Delta_2-\nabla_z^2\right)\nabla_z w+\overline{H}_2\left(\Delta_2+\partial_z^2\right)\nabla_z w \qquad (4.25)\\
\partial_t\theta-w &= \nabla_z^2\theta+\alpha\Delta_2\theta \qquad (4.26)
\end{aligned}$$

with the 2-dimensional Laplace operator $\Delta_2=(\nabla_x^2+\nabla_y^2)$. The material dependent coefficients are $a=(\nu_3+\frac{1}{4}\gamma(1+\lambda)^2)/\nu_2$, $b=(2\nu_1+2\nu_2-2\nu_3+\frac{\gamma_1}{2}(\lambda^2+1))/\nu_2$, $c=(\nu_3+\frac{1}{4}\gamma(1-\lambda)^2)/\nu_2$, $d=\bar{\nu}_1^R/\bar{\nu}_2^R$, $e=\bar{\nu}_3^R/\bar{\nu}_2^R$, and $\alpha=\kappa_\parallel/\kappa\perp$, with Ra the Rayleigh number $Ra=gd^3\alpha_p(T_0-T_1)/(\nu_2 k_\perp)$ and Pr the Prandtl number $Pr=\nu_2/k_\perp$. The magnetic field enters in the non-dimensional form $\overline{H}_1=\bar{\nu}_2^R H/\nu_2$ and $\overline{H}_2=\bar{\bar{\nu}}^R H/\nu_2$.

One can see that in addition to the degrees of freedom that are necessary to describe the Rayleigh-Bénard instability in usual nematics, there is also ξ, the z - component of the vorticity. This situation is similar to the case of the thermal instability in a rotating layer of simple liquids [74]. In both cases the time reversal symmetry is broken by the external (flow or magnetic) field. In our geometry we expect a roll pattern due to the spatial up-down or mid-plane symmetry that is still present. In such a pattern the z-component of the vorticity is manifest as a crossflow in the $x-y$ plane as shown in Fig. 4.2. Measuring this component of the velocity can serve as a direct indication of the presence of the new field-dependent terms in the viscosity tensor. Although ferrofluids are rather dark and flow is difficult to view directly, reflecting tracer particles may be used.

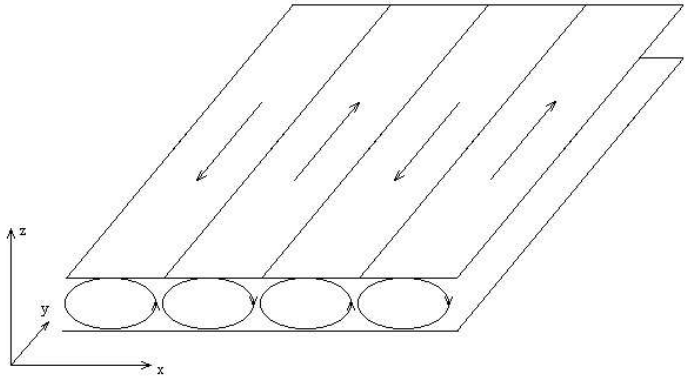

Figure 4.2: The effect of the new field-dependent terms in the effective viscosity tensor on the convection roll pattern. The flow due to the non-zero vorticity component is shown by arrows on the top; at the bottom the arrows are in opposite direction. The orientation of the rolls is chosen to be the y-direction, arbitrarily.

We have determined the threshold of the stationary instability taking for example the material parameters of MBBA liquid crystals. Assuming non-slip boundary condition we use the

method suggested in [75] (cf. App. 2.6.1). On Fig. 4.3 one can see the threshold as a function of the non-dimensional magnetic field $\overline{H} = \overline{H}_1 + \overline{H}_2 = H(\nu_4^R + \nu_5^R + \nu_7^R + 3\nu_8^R)/\nu_2$ for the case $\bar{\nu}_1^R = \bar{\nu}_2^R = \bar{\nu}_3^R = \bar{\nu}_4^R = \bar{\bar{\nu}}^R$ (this additional assumption is made for representative reasons only). For low fields the threshold is a quadratic function of the magnetic field, which is to be expected, since the Rayleigh number is a scalar while the magnetic field is a vector. This quadratic field dependence is not specific for the new contributions in the viscosity tensor, since any (trivial) H^2-dependence of material parameters would produce such an effect. The $\overline{H}$ effect on Ra_c is rather small. In order to get a 3% increase, $\overline{H}$ has to be about 0.5 requiring the field H and the typical ν_α^R to be so large that $H\nu_\alpha^R$ is about one order of magnitude smaller than the ordinary shear viscosity ν_2.

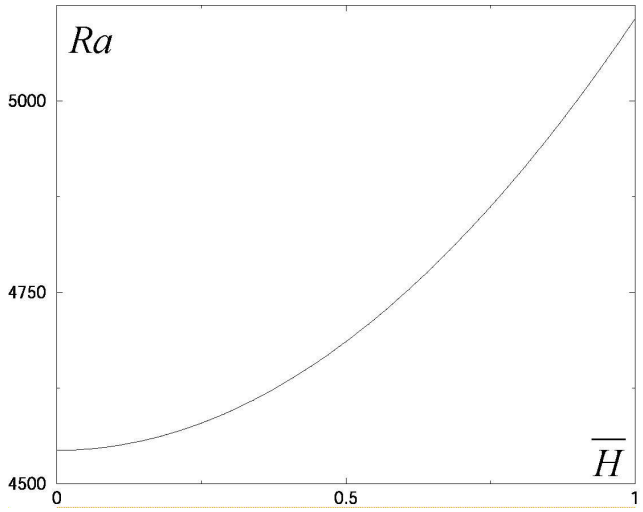

Figure 4.3: The critical Rayleigh number Ra_c as a function of the magnetic field $\overline{H}$ (parallel case).

The high value of the threshold without field is due to our assumption of quenched director orientation, which leads to the presence of the additional terms $\lambda_{pji}^R \gamma_{pm}^D \lambda_{mkl}^R$ in the viscosity tensor (4.13). For very high fields, which are probably beyond experimental reach, $Ra_c \sim \overline{H}^{4/3}$, asymptotically. Comparing with the case of a Rayleigh-Bénard experiment under rotation in simple fluids [74], where an oscillatory instability is possible for very low Prandtl numbers, we expect the instability to be always stationary here, since $Pr \gg 1$ in nematics. In the rotation case, the stationary rolls are known to be subject to the Küppers-Lortz secondary instability into a non-stationary state at even higher Rayleigh number $Ra > Ra_c$ [93], and this behavior can be expected here in the ferronematic case, too.

4.3.2 The case when $\boldsymbol{n} \perp \boldsymbol{H}$

When the magnetic susceptibility anisotropy is negative $\chi_a < 0$, the director field tends to be perpendicular to the magnetic field. This is the typical case for lyotropic systems. Here, in principle also concentration and mixture effects have to be taken into account. In the preceding chapters we have shown their importance for isotropic ferrofluids. Here we concentrate on the

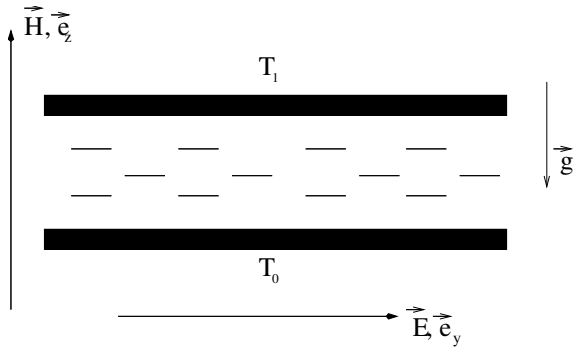

Figure 4.4: Sketch of the setup in the perpendicular case. For details see text.

qualitatively new linear magnetic field effects that are independent from the binary mixture behavior and stick to the simplified single-component description.

To consider the influence of the new magnetic field dependent terms we consider the geometry shown in Fig. 4.4. As in the previous case we have an infinite layer of ferronematics subject to a temperature gradient across the layer. An external magnetic field is imposed along the temperature gradient (z-direction,) while the nematic director is oriented perpendicular (y-direction). We assume that also a strong electric field is applied, in order to clamp the director in its equilibrium orientation. Thus, like in the preceding section, director reorientations are neglected. In this case the equations describing linear stability analysis are again given by Eqs. (4.20-4.22), where the effective viscosity tensor (4.13) now takes the form (4.42) given in App. 4.6.2.

We also assume that the magnetic field dependent contributions come only from the viscosity tensor, i.e. we neglect all λ_α^D in (4.43). Otherwise we need to explore a parameter space of very high dimension. This is not reasonable at present, since those parameters are unknown and we are interested in qualitative effects only. In this case the magnetic field enters the equations through two material dependent dimensionless coefficients

$$\begin{aligned} \overline{H}_1 &= (\nu_2^R - \nu_7^R + \nu_8^R)H/\nu_2 \\ \overline{H}_2 &= (\nu_1^R + \nu_2^R - 2\nu_5^R - \nu_7^R - 3\nu_8^R)H/\nu_2 \end{aligned} \tag{4.27}$$

which contain combinations of the ν_α^R ($\alpha = 1...8$) introduced in [57]. If no magnetic field is present, the behavior of the system is that of a pure simple liquid and the convection sets in at $Ra_c = 1708$, because the heat focusing effect of nematics [94] is suppressed by clamping the director. Comparing with the case $\boldsymbol{n} \parallel \boldsymbol{H}$ the clamped nematic degree of freedom now is inoperative with respect to the onset of the instability, but sets the direction of the rolls.

If we switch on the external magnetic field, the new dynamic field-dependent terms come into play and the instability picture changes considerably. To study this problem in more detail we use a three dimensional analysis introduced in [95]. The velocity field is represented by two scalar potentials f and g

$$\boldsymbol{v} = \begin{pmatrix} \nabla_x\nabla_z f + \nabla_y g \\ \nabla_y\nabla_z f - \nabla_x g \\ -\nabla_x\nabla_x f - \nabla_y\nabla_y f \end{pmatrix} \tag{4.28}$$

Due to the homogeneity in the lateral directions we can take all fields to be of the form $\{f, g, \theta\} = \{f(z), g(z), \theta(z)\}exp\{i\boldsymbol{kr} + i\omega t\}$, where $\boldsymbol{k}$ is a two-dimensional wave vector in the

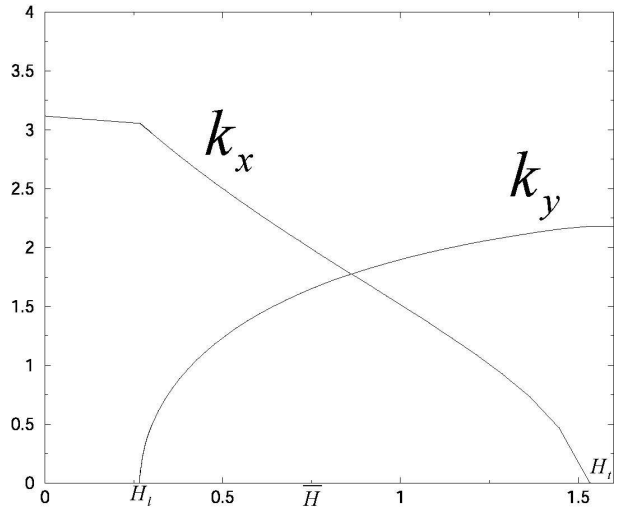

Figure 4.5: The wave vector components k_x and k_y corresponding to the minimum of the function $Ra_c(k_x, k_y)$ as a function of the magnetic field $\overline{H}$.

$x - y$ plane. Substituting (4.28) into the linearized equations (4.20-4.22) and taking $curl_z$ as well as $(curl\, curl)_z$ of (4.20) we get the linear system of equations

$$\hat{L}(Ra, k_x, k_y, \omega, \overline{H}_1, \overline{H}_2) \begin{pmatrix} f \\ g \\ \theta \end{pmatrix} = 0 \tag{4.29}$$

where $\hat{L}$ is a linear differential operator of eighth order with respect to z. The explicit form of Eqs. (4.29) is presented in (4.44-4.46) in App. 4.6.3. No-slip boundary conditions translate into

$$\begin{aligned} f(0) = f(1) = f'(0) = f'(1) &= 0 \\ g(0) = g(1) &= 0 \\ \theta(0) = \theta(1) &= 0 \end{aligned} \tag{4.30}$$

To find the threshold of a stationary instability we take $\omega = 0$. At any given values of k_x, k_y, $\overline{H}_1$,and $\overline{H}_2$ the problem is to find the value Ra such that the boundary value problem (4.29-4.30) has a nontrivial solution. The function $Ra(k_x, k_y)$ is then minimized to find the threshold Ra_c for the given values of $\overline{H}_1$ and $\overline{H}_2$.

The solution of this problem was accomplished using the shooting method presented in Ref. [75] (cf. App. 2.6.1). Here the system of linear differential equations is solved using a matrix representation of the solution. The parameters were taken as those for MBBA liquid crystals. In order to simplify the presentations of the results we take $\overline{H}_2 = 0$ ($\overline{H}_1 = \overline{H}$). This additional assumption does not change the qualitative picture of the instability, nor does it affect the limiting cases $H = 0$ and $H \to \infty$. In the case of zero magnetic field the minimum of the function $Ra(k_x, k_y)$ is on the line $k_y = 0$, which corresponds to rolls aligned along the nematic director. The critical Rayleigh number is then $Ra_c = 1708$ as expected [94]. Increasing slightly the strength of the magnetic field leads to an increase in Ra_c, but k_y is still zero. When the value of $\overline{H}$ exceeds some critical value $\overline{H}_\ell$ the minimum of the function $Ra(k_x, k_y)$ shifts to

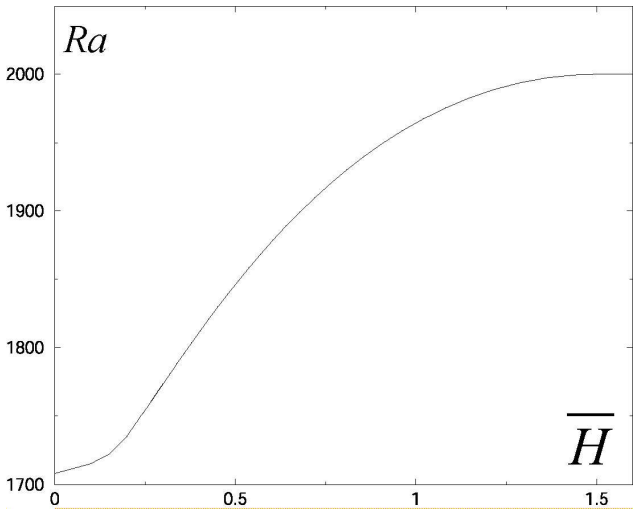

Figure 4.6: The critical Rayleigh number Ra_c as a function of the magnetic field $\overline{H}$ (perpendicular case).

a finite $k_y \neq 0$. On Fig. 4.5 the dependence of k_x and k_y on $\overline{H}$ is presented. The appearance of a finite k_y above $\overline{H}_\ell$ is accompanied by a strong drop of k_x. The critical $\overline{H}_\ell$ already corresponds to a rather large field H, for which the product with a typical ν_α^R, $H\nu_\alpha^R$, is almost of the order of the shear viscosity ν_2.

When the magnetic field is increased further above $\overline{H}_t$, we get finally $k_x = 0$. The minimum of $Ra(k_x, k_y)$ is then along the line $k_x = 0$ and the rolls are aligned perpendicular to the director. Any further increase of $\overline{H}$ does not change the position of the rolls, nor the value of the critical Rayleigh number. The threshold value as a function of the magnetic field is presented in Fig. 4.6.

Analyzing these results we can predict the corresponding flow patterns. First, when $\overline{H} < \overline{H}_\ell$ the convective rolls are aligned along the electric field. When the magnetic field exceeds this lower critical value $\overline{H}_\ell$, the rolls get oblique with respect to the electric field and the angle between the rolls and the electric field increases with increasing magnetic field. At the point when the magnetic field reaches the upper critical value H_t, the rolls are perpendicular to the electric field and stay so for any higher field. Note that the director is always parallel to the electric field (and perpendicular the external magnetic field). Thus, in the intermediate magnetic field regime the director is oblique to the roll orientation, while in the high field regime it is perpendicular. It is possible that this high field regime cannot be reached in actual experiments.

We have looked numerically for an oscillatory instability, but did not find any. Since this search could be done for a limited parameter range only, this is no proof for a general absence of an oscillatory instability. In principle, the set of equations (4.29,4.30) can support non-trivial solutions at a finite frequency $\omega \neq 0$, since it is not self-adjoint.

4.4 Saffman-Taylor instability

Another useful tool to study the new linear field dependent contributions in the effective viscosity tensor is flow in a Hele-Shaw cell. When a viscous fluid is displaced by a less viscous one in the narrow space of a Hele-Shaw cell the Saffman-Taylor instability arises [96]. We consider a radial Hele-Shaw cell (Fig. 4.7), which consists of two parallel transparent plates at a distance d. The gap between them is filled with a high viscosity fluid, in our case a ferronematic. The low viscosity one (usually air) is injected through an inlet at the center of the upper plate.

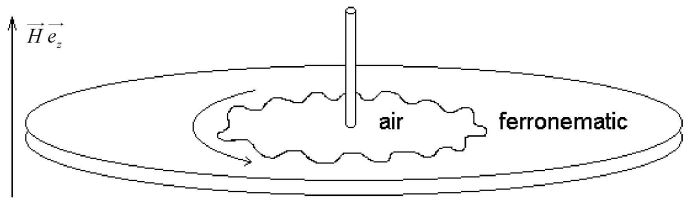

Figure 4.7: The setup of a radial Hele-Shaw cell. For a ferronematic the external magnetic field leads to the rotation of the fingers shown by the arrow.

A magnetic field is imposed perpendicular to the plates (in z-direction) strong enough for the nematic director to be clamped. Here we again assume that the magnetic susceptibility anisotropy is positive and the director field is aligned parallel to the external field.

The description of the fluid motion far from the interface follows the usual lines [97]. Neglecting the inertia terms in the Navier-Stokes equation (4.11) we have

$$\nabla_i p = \rho_0 \, \mu^{eff}_{ijkl} \, \nabla_j \nabla_k \, v_l \tag{4.31}$$

where $\rho_0 \mu^{eff}_{ijkl}$ is given by (4.23) and the pressure gradient is constant along the radial directions. Since the gap d is small, we can neglect all derivatives of the velocity except those along the z-direction. Integrating (4.31) twice and taking the mean with respect to z-direction we get a linear relation between the mean velocity and the pressure gradient

$$v_i \;=\; -\frac{d^2}{12(A^2_{eff} + B^2_{eff})}(A_{eff}\delta_{ij} - B_{eff}\epsilon_{ijz})\nabla_j p \tag{4.32}$$

with $A_{eff} = \nu_3 + \frac{1}{4}\gamma(1-\lambda)^2$ and $B_{eff} = H(\bar{\nu}^R_2 + \bar{\bar{\nu}}^R)$, where $\bar{\nu}^R_2$ and $\bar{\bar{\nu}}^R$ are given in Eq. (4.41). In cylindrical coordinates (r, θ, z) there is – apart from the usual radial component of the mean velocity v_r parallel to the pressure gradient – now also an azimuthal mean velocity component

v_θ perpendicular to the pressure gradient, due to the new linear field terms in the effective viscosity tensor.

We will now consider how this azimuthal component of the velocity changes the picture of the Saffman-Taylor instability in the radial Hele-Shaw cell. Without perturbations the interface between the ferronematic liquid and the air is a circle with radius $R(t)$ (measured from the point of injection) that increases in time according to the radial velocity (normal to the interface) $v_n = v_r$. The tangential velocity, can be related to the normal one

$$v_T = v_\theta = \frac{B_{eff}}{A_{eff}} v_n \tag{4.33}$$

We investigate the linear stability of this interface with respect to azimuthal shape distortions ("fingers") by assuming the interface to be located at $r(\theta, t) = R(t) + \zeta(\theta, t)$, with small perturbations $\zeta(\theta, t)$. The time evolution of these perturbations is related to perturbations, δv_n, in the normal velocity by the linearized kinematic condition

$$\partial_t \zeta + v_T \nabla_T \zeta = \delta v_n \tag{4.34}$$

taken at the undistorted interface $R(t)$. Here the tangential velocity v_T enters, since the distorted interface is no longer circular. Since the function $\zeta(\theta, t)$ has to be periodic in θ in order to have a well-defined interface, we can decompose it into discrete modes

$$\zeta(\theta, t) = \sum_{m=1}^{m=\infty} \zeta_m(t)\, \cos(m\theta + \phi_m(t)) \tag{4.35}$$

and make the linear stability analysis for each Fourier mode separately. We have allowed for a (still unknown) phase $\phi_m(t)$ for each mode. For the perturbations of the normal velocity we can write in linear approximation

$$\delta v_n = \sum_{m=1}^{m=\infty} \zeta_m(t) \widehat{\mu_m}(\theta, t) \cos(m\theta + \phi(t)) \tag{4.36}$$

where $\widehat{\mu_m}(\theta, t)$ is an operator with respect to θ. The actual form of this operator depends on the details of the boundary conditions [98]. We will assume for simplicity that $\widehat{\mu_m}(\theta, t)$ is independent of v_T. This is justified as long as the interface forces are not drasticaly altered by the magnetic field. Then it has the usual form

$$\widehat{\mu_m}(\theta, t) = a(R(t), m) + b(R(t), m) \frac{\partial^2}{\partial \theta^2} \tag{4.37}$$

where the explicit expressions for the functions $a(m)$ and $b(m)$ are rather involved and are the subject of special investigations (see for example [99]) due to the non-trivial physical mechanism involving the capillary force. However, since we are interested in the qualitatively new effects due to the finite tangential velocity v_T, the special form of $a(m)$ and $b(m)$ is unimportant here.

Substituting (4.35) and (4.36) into (4.34) and taking into account (4.37) we get for ζ_m and ϕ_m

$$\dot{\zeta}_m(t) = -\mu_m(t)\, \zeta_m(t) \tag{4.38}$$

$$\dot{\phi}_m = -m \frac{v_T}{R(t)} \tag{4.39}$$

where v_T is taken at $R(t)$. Here $\mu_m \equiv -a(R(t), m) + m^2\, b(R(t), m) = 0$ defines implicitly the most unstable mode. This pattern of fingers is rotating with angular velocity $mv_T/R(t)$ due to the time evolution of the phase $\phi(t)$. Within our assumptions the phase evolution (4.39) is completely decoupled from that of the amplitude and the details of $a(m)$ and $b(m)$ are unimportant. The amplitude equation (4.38) is independent of the new viscosity contributions and all previous investigations of the Saffman-Taylor instabilities for simple nematic liquid crystal (see for example [96]) are valid in this respect also for ferronematics. But in addition to the amplitude amplification there is the rotation of the growing fingers with angular velocity

$$\dot{\phi}_m = -\frac{mQ}{2\pi R(t)^2 d}\,\frac{B_{eff}}{A_{eff}} \tag{4.40}$$

where we have used Eq. (4.33) to express v_T by v_n. The flow rate of the injected air, Q, is related to the normal velocity of the interface by $Q = 2\pi d\, R(t)\, v_n$. Note that the sense of rotation reverses, if the magnetic field is inverted. The rotation velocity slows down with increasing interface radius $R(t)$ and is larger for a narrower gap.

4.5 Conclusions (Chap. 4)

We have discussed typical hydrodynamic instabilities in ferronematics under the aspect of qualitatively new effects due to the linear magnetic-field contributions to the dynamics of those materials. In Rayleigh-Bénard instabilities with the temperature gradient adverse to gravity we find, in addition to convection flow in the form of one-dimensional rolls, a vorticity flow. As a consequence, in the homeotropic case (the director parallel to the field) the streamlines are oblique to the roll cross-section, while in the planar case (the director perpendicular to the magnetic, but parallel to an electric field) the rolls themselves are tilted with respect to the director depending on the magnetic field strength. In the Saffman-Taylor viscous fingering instability of a growing interface between fluids of different density, the new linear magnetic-field contributions lead to a rotation of the finger structure. Since the new effects are linear in the external field and therefore change sign when the field is inverted, they are clearly distinct from those effects that are based on the intrinsic field dependence of conventional transport parameters, which are quadratic in the field. All these effects exist in principle in any nematic liquid crystal, since they are connected to the nematic degree of freedom, only, and not to the magnetization as an independent variable. In ordinary nematics, however, the interaction with magnetic fields is very weak and those effects have never been observed. In ferronematics, where the static response to magnetic fields is known to be enhanced by several orders of magnitude, one can expect that the influence of the magnetic field on the dynamics is also increased and strong enough to make the effects described here measurable.

4.6 Appendix (Chap. 4)

4.6.1 The form of the coefficients $\bar{\nu}_\alpha^R$ and $\bar{\bar{\nu}}^R$

Here we express the abbreviations $\bar{\nu}_\alpha^R$ and $\bar{\bar{\nu}}^R$ introduced in (4.23) by the coefficients introduced in [57]:

$$\begin{aligned}
\bar{\nu}_1^R &= \nu_4^R + \nu_5^R + 2\nu_8^R - \frac{\gamma_1^2}{4}\left(\frac{1}{\gamma_1^R} + \frac{1}{\gamma_2^R}\right)\left(\lambda^2 - 1\right) - \frac{\gamma_1}{2}\left(\lambda_1^D + \lambda_3^D + \lambda_4^D\right)\lambda \\
\bar{\nu}_2^R &= \nu_4^R + \nu_5^R + 2\nu_8^R - \frac{\gamma_1^2}{4}\left(\frac{1}{\gamma_1^R} + \frac{1}{\gamma_2^R}\right)(\lambda+1)^2 - \frac{\gamma_1}{2}\left(\lambda_1^D + \lambda_3^D + \lambda_4^D\right)(\lambda+1) \\
\bar{\nu}_3^R &= \bar{\nu}_1^R \\
\bar{\nu}_4^R &= \nu_4^R + \nu_5^R + 2\nu_8^R - \frac{\gamma_1^2}{4}\left(\frac{1}{\gamma_1^R} + \frac{1}{\gamma_2^R}\right)(\lambda-1)^2 - \frac{\gamma_1}{2}\left(\lambda_1^D + \lambda_3^D + \lambda_4^D\right)(\lambda-1) \\
\bar{\bar{\nu}}^R &= \nu_7^R + \nu_6^R
\end{aligned} \tag{4.41}$$

4.6.2 The effective viscosity tensor in the case when $\boldsymbol{n} \perp \boldsymbol{H}$

With $\boldsymbol{H} = H\boldsymbol{e}_z$ and $n_i = \delta_{iy}$ we get

$$\begin{aligned}
\rho_0\,\mu_{ijkl}^{eff} &= \nu_2\left(\delta_{jl}\delta_{ik} + \delta_{il}\delta_{jk}\right) \\
&\quad +2(\nu_1 + \nu_2 - 2\nu_3 + \tfrac{1}{2}\gamma_1\lambda^2)\, n_i n_j n_k n_l \\
&\quad +(\nu_3 - \nu_2)(n_j n_l \delta_{ik} + n_j n_k \delta_{il} + n_i n_k \delta_{jl} + n_i n_l \delta_{jk}) \\
&\quad +\tfrac{1}{4}\gamma_1\left((\lambda-1)^2\delta_{jk}n_i n_l + (\lambda+1)^2\delta_{il}n_j n_k + (\lambda^2-1)(\delta_{jl}n_i n_k + \delta_{ik}n_j n_l)\right) \\
&\quad -H\,(\hat{\nu}_{1a}^R\delta_{ix}n_j n_k n_l + \hat{\nu}_{1b}^R\delta_{jx}n_i n_k n_l - \hat{\nu}_{1b}^R\delta_{kx}n_j n_i n_l - \hat{\nu}_{1a}^R\delta_{lx}n_j n_k n_i \\
&\qquad +\hat{\nu}_{2a}^R\delta_{jx}n_l\delta_{ik} - \hat{\nu}_{2b}^R\delta_{lx}n_j\delta_{ik} + \hat{\nu}_{2b}^R\delta_{jx}n_k\delta_{il} - \hat{\nu}_{2b}^R\delta_{kx}n_j\delta_{il} \\
&\qquad +\hat{\nu}_{2b}^R\delta_{ix}n_k\delta_{jl} - \hat{\nu}_{2a}^R\delta_{kx}n_i\delta_{jl} + \hat{\nu}_{2a}^R\delta_{ix}n_l\delta_{jk} - \hat{\nu}_{2a}^R\delta_{lx}n_i\delta_{jk} \\
&\qquad +\hat{\nu}_{3a}^R\delta_{kx}n_l\delta_{ij} + \hat{\nu}_{3b}^R\delta_{lx}n_k\delta_{ij} - \hat{\nu}_{3b}^R\delta_{ix}n_j\delta_{kl} - \hat{\nu}_{3a}^R\delta_{jx}n_i\delta_{kl}) \\
&\quad +\nu_5^R H\left(\varepsilon_{ikz}n_j n_l + \varepsilon_{ilz}n_j n_k + \varepsilon_{jlz}n_i n_k + \varepsilon_{jkz}n_i n_l\right) \\
&\quad +\nu_7^R H\left(\varepsilon_{ikz}\delta_{jl} + \varepsilon_{ilz}\delta_{jk} + \varepsilon_{jlz}\delta_{ik} + \varepsilon_{jkz}\delta_{il}\right) \\
&\quad +H\left(\hat{\nu}_{8a}^R\varepsilon_{iky}\left(\delta_{jz}n_l + \delta_{lz}n_j\right) + \hat{\nu}_{8b}^R\varepsilon_{ily}\left(\delta_{jz}n_k + \delta_{kz}n_j\right)\right. \\
&\qquad \left.+\hat{\nu}_{8c}^R\varepsilon_{jly}(\delta_{iz}n_k + \delta_{kz}n_i) + \hat{\nu}_{8d}^R\varepsilon_{jky}(\delta_{iz}n_l + \delta_{lz}n_i)\right)
\end{aligned} \tag{4.42}$$

with the abbreviations

$$
\begin{aligned}
\hat{\nu}_{1a}^R &= \nu_1^R - \frac{\gamma_1}{4}\left((2\lambda_1^D - \lambda_5^D + \lambda_6^D)(\lambda+1) - 2\lambda_2^D\lambda\right)\\
\hat{\nu}_{1b}^R &= \nu_1^R - \frac{\gamma_1}{4}\left((2\lambda_1^D - \lambda_5^D + \lambda_6^D)(\lambda-1) - 2\lambda_2^D\lambda\right)\\
\hat{\nu}_{2a}^R &= \nu_2^R - \frac{\gamma_1}{4}(\lambda-1)\lambda_2^D\\
\hat{\nu}_{2b}^R &= \nu_2^R - \frac{\gamma_1}{4}(\lambda+1)\lambda_2^D\\
\hat{\nu}_{3a}^R &= \nu_3^R + \frac{\gamma_1}{4}(\lambda-1)\lambda_6^D\\
\hat{\nu}_{3b}^R &= \nu_3^R + \frac{\gamma_1}{4}(\lambda+1)\lambda_6^D\\
\hat{\nu}_{8a}^R &= \nu_8^R + \frac{\gamma_1}{4}2\lambda_3^D\\
\hat{\nu}_{8b}^R &= \nu_8^R + \frac{\gamma_1}{4}(\lambda+1)\lambda_3^D\\
\hat{\nu}_{8c}^R &= \hat{\nu}_{8a}^R\\
\hat{\nu}_{8d}^R &= \nu_8^R + \frac{\gamma_1}{4}(\lambda-1)\lambda_3^D
\end{aligned}
\tag{4.43}
$$

4.6.3 The linear stability problem in the case when $\boldsymbol{n} \perp \boldsymbol{H}$

In this appendix we present the explicit form of the linear stability problem for the case when $\boldsymbol{n} \perp \boldsymbol{H}$. It can be expressed in the form (4.29):

$$
\begin{aligned}
i\omega\left(k_x^2+k_y^2\right)\left(k_x^2+k_y^2-\frac{d^2}{dz^2}\right)f \;=\; & -\left(\left(\frac{\gamma_1}{4}\left(\lambda-1\right)^2+\nu_3\right)k_x^2+\nu_2 k_y^2\right)f^{IV}\\
& +\left(2\nu_2+2\nu_3+\frac{\gamma_1}{2}\left(1+\lambda^2\right)\right)k_x^2k_y^2\,f''\\
& +\left(\left(2\nu_1+2\nu_2-3\nu_3-\frac{\gamma_1}{2}\left(\lambda^2-1\right)\right)k_x^4+2\nu_2k_y^4\right)f''\\
& -\left(\left(\frac{\gamma_1}{4}\left(1+\lambda\right)^2+\nu_3\right)k_x^6+\nu_2k_y^6\right)f\\
& -\left(\frac{\gamma_1}{2}\left(1+\lambda\right)^2+\nu_2+2\nu_3\right)k_x^4k_y^2\,f\\
& -\left(\frac{\gamma_1}{4}\left(1+\lambda\right)^2+2\nu_2+\nu_3\right)k_x^2k_y^4\,f\\
& +\left(\frac{\gamma_1}{4}\left(\lambda-1\right)^2-\nu_2+\nu_3\right)k_xk_y\,g'''\\
& -\left(\frac{\gamma_1}{4}\left(1-2\lambda-3\lambda^2\right)+2\nu_1+\nu_2-3\nu_3\right)k_x^3k_y\,g'\\
& -\left(\frac{\gamma_1}{4}\left(\lambda-1\right)^2-\nu_2+\nu_3\right)k_xk_y^3\,g'\\
& +ik_y\left(k_x^2+k_y^2\right)\left(\left(\overline{H}_2k_x^2+\overline{H}_1k_y^2\right)g-\overline{H}_1\,g''\right)\\
& +(k_x^2+k_y^2)\mathrm{g}\alpha_p\,\theta
\end{aligned}
\tag{4.44}
$$

$$
\begin{aligned}
i\omega\left(k_x^2+k_y^2\right)g \;=\; & -\left(\frac{\gamma_1}{4}\left(\lambda-1\right)^2-\nu_2+\nu_3\right)k_xk_y\,f''' \\
& +\left(\frac{\gamma_1}{4}\left(\lambda-1\right)^2-\nu_2+\nu_3\right)k_y^2\,f' \\
& -\left(\frac{\gamma_1}{4}\left(3\lambda-1\right)\left(1+\lambda\right)-\nu_1-\nu_2+3\nu_3\right)k_xk_y\,f' \\
& +\left(\left(\frac{\gamma_1}{4}\left(\lambda-1\right)^2+\nu_3\right)k_y^2+\nu_2k_x\right)g'' \\
& -\left(\frac{\gamma_1}{4}\left(k_y^2(\lambda-1)+k_x^2(1+\lambda)\right)^2\right)g \\
& -\left(k_x^2k_y^2\left(2\nu_1+2\nu_2\right)-\nu_3\left(k_x^2-k_y^2\right)^2\right)g \\
& +ik_y(k_x^2+k_y^2)\left(\left(\overline{H}_2k_y^2+\overline{H}_1k_x^2\right)f-\overline{H}_1\,f''\right)
\end{aligned}
\tag{4.45}
$$

$$
i\omega\theta \;=\; \kappa_\perp\theta''-\left(\kappa_\perp k_y^2+\left(\kappa_\parallel+\kappa_\perp\right)k_x^2\right)\theta+\frac{T_0-T_1}{h}(k_x^2+k_y^2)f \tag{4.46}
$$

Bibliography

[1] R.E. Rosensweig, *Ferrohydrodynamics*, Cambridge University Press, Cambridge, 1985.

[2] C. Alexiou, W. Arnold, R.J. Klein, F.G. Parak, P. Hulin, C. Bergemann, W. Erhardt, S. Wagenpfeil, and A.S. Lübbe, *Cancer Research* **60** (2000) 6641.

[3] I. Hilger, R. Hiergeist, K. Hergt, H. Winnefeld, H. Schubert, and W.A. Keiser, *Investigative Radiology* **37** (2002) 580.

[4] J.-C. Bacri, U. d'Ortona, and D. Salin, *Phys. Rev. Lett.* **67** (1991) 50.

[5] J.-C. Bacri, A. Cerbers, J.-C. Dabadie, and R. Perzynski, *Europhys. Lett.* **27** (1994) 437.

[6] J.-C. Bacri, A. Cerbers, J.-C. Dabadie, and R. Perzynski, *Phys. Rev.* **E 50** (1994) 2712.

[7] B.A. Finlayson, *J. Fluid Mech.* **40** (1970) 753.

[8] L. Schwab, U. Hildebrandt, and K. Stierstadt, *J. Magn. Magn. Mater.* **39** (1983) 113; L. Schwab, *Konvektion in Ferrofluiden*, PhD thesis, Munich 1989.

[9] A. Ryskin, H.-W. Müller, and H. Pleiner, *Phys. Rev.* **E 67** (2003) 046302; *Magnetohydrodynamics* **39** (2003) 51.

[10] A. Ryskin and H. Pleiner, submitted to *Phys.Rev.* **E**.

[11] M.I. Shliomis and M. Souhar, *Europhys. Lett.* **49** (2000) 55.

[12] S. Odenbach and H. Gilly, *J. Magn. Magn. Mater.* **152** (1996) 123.

[13] M. Niklas, H. Müller-Krumbhaar, and M. Lücke, *J. Magn. Magn. Mater.* **81** (1989) 29.

[14] M. Niklas, *Z. Phys. B: Condens. Matter* **68** (1987) 493.

[15] D.P. Jackson, R.E. Goldstein, A.O. Cerbers, *Phys. Rev.* **E 50** (1994) 298.

[16] J.A. Miranda, *Phys. Rev.* **E 62** (2000) 2985.

[17] I. Dirkis and A. Cerbers, *J. Magn. Magn. Mater.* **201** (1999) 339

[18] Z. Wang, C. Holm, and H.-W. Müller, *Phys. Rev.* **E 66** (2002) 021405.

[19] M. Kröger, P. Ilg, and S. Hess, *J. Phys.: Condens. Matter* **15** (2003) S1403.

[20] A.Yu. Zubarev, S. Odenbach, and J. Fleischer *J. Magn. Magn. Mater.* **252** (2002) 241.

[21] S. Odenbach, T. Rylewicz, and M. Heyen, *J. Magn. Magn. Mater.* **201** (1999) 155.

[22] H.-W. Müller and M. Liu, *Phys. Rev.* **E 64** (2001) 061405.

[23] J. Lenglet, A. Bourdon, J.-C. Bacri, and G. Demouchy, *Phys. Rev.* **E 65** (2002) 031408.

[24] B.V. Derjaguin, S.S. Dukhin, and A.A. Korotkova, *Kolloidn. Zh.* **23** (1961) 53.

[25] J.K. Platten and J.C. Legros, *Convection in Liquids*, Springer, Berlin, 1984.

[26] M.C. Cross and P.C. Hohenberg, *Rev. Mod. Phys.* **49** (1993) 581.

[27] M. Lücke, W. Barten, P. Büchel, C. Fütterer, St. Hollinger, and Ch. Jung, *Pattern formation in binary fluid convection and in systems with throughflow*, in *Evolution of Spontaneous Structures in Continuous Systems* (eds. F.H. Busse and S.C. Müller), Springer, Berlin. Lecture Notes in Physics **55** (1998) 127.

[28] B. Huke, M. Lücke, P. Büchel, and Ch. Jung, *J. Fluid Mech.* **408** (2000) 121.

[29] E. Moses and V. Steinberg, *Phys. Rev.* **A 43** (1991) 707.

[30] H.-W. Müller and M. Lücke, *Phys. Rev.* **A 38** (1988) 2965.

[31] Ch. Jung, B. Huke and M. Lücke *Phys. Rev. Lett.* **81** (1998) 3651.

[32] R.W. Walden, P. Kolodner, A. Passner, and C.M. Surko, *Phys. Rev. Lett.* **55** (1985) 496.

[33] W. Barten, M. Lücke, W. Hort, and M. Kamps, *Phys. Rev. Lett.* **63** (1989) 376.

[34] D. Jung and M. Lücke, *Phys. Rev. Lett.* **89** (2002) 054502.

[35] C. Fütterer and M. Lücke, *Phys. Rev.* **E 65** (2002) 036315.

[36] P. Büchel and M. Lücke, *Phys. Rev.* **E 63** (2002) 016307.

[37] F. Brochard and P.G. de Gennes, *J. Phys. (France)* **31** (1970) 691.

[38] J. Rault, P.E. Cladis, and J.P. Burger, *Phys. Lett.* **A 32** (1970) 199.

[39] C.F. Hayes, *Mol. Cryst. Liq. Cryst.* **36** (1976) 245.

[40] L. Liébert and A. Martinet, *J. Phys. Lett.(France)* **40** (1979) 363.

[41] S.-H. Chen and S.H. Chiang, *Mol. Cryst. Liq. Cryst.* **144** (1987) 359.

[42] P. Fabre, C. Casagrande, M. Veyssié, V. Cabuil, and R. Massart, *Phys. Rev. Lett.* **64** (1990) 539.

[43] J.C. Dabadie, P. Fabre, M. Veyssié, V. Cabuil, and R. Massart, *J. Phys: Condens. Matter* **2**, Suppl. A (1990) SA291.

[44] V. Ponsinet, P. Fabre, and M. Veyssié, *Europhys. Lett.* **30** (1995) 277.

[45] D. Spoliansky, J. Ferré, J.-P. Jamet, and V. Ponsinet, *J. Magn. Magn. Mater.* **201** (1999) 200.

[46] J.C. Bacri, V. Cabul, A. Cebers, C. Menager, and R. Perzynski, *Europhys. Lett.* **33** (1996) 235.

[47] J.C. Bacri and A.M. Figueiredo Neto, *Phys. Rev.* **E 50** (1994) 3860.

[48] S.I. Burylov and Y.L. Raikher, *Mol. Cryst. Liq. Cryst.* **258** (1995) 123.

[49] Y.L. Raikher and V.I. Stepanov, *J. Magn. Magn. Mater.* **201** (1999) 182.

[50] I. Potočová, M. Koneracká, P. Kopčanský, M. Timko, L. Tomčo, J. Jadżyn, and G. Czechowski, *J. Magn. Magn. Mater.* **196** (1999) 578.

[51] M. Koneracká, V. Závišová, P. Kopčanský, J. Jadżyn, G. Czechowski, and B. Żywucki, *J. Magn. Magn. Mater.* **157/158** (1996) 589.

[52] V. Berejnov, J.-C. Bacri, V. Cabuil, R. Perzynski, and Y.L. Raikher, *Europhys. Lett.* **41** (1998) 507.

[53] A.Yu. Zubarev and L.Yu. Iskakova, *J. Magn. Magn. Mater.* **183** (1998) 201.

[54] C.Y. Matuo and A.M. Figueiredo Neto, *Phys. Rev.* **E 60** (1999) 1815.

[55] S. Fontanini, A.L. Alexe-Ionescu, G. Barbero, and A.M. Figueiredo Neto, *J. Chem. Phys.* **106** (1997) 6187.

[56] S.-H. Chen and N.M. Amer, *Phys. Rev. Lett.* **51** (1983) 2298.

[57] E. Jarkova, H. Pleiner, H.-W. Müller, A. Fink, and H.R. Brand, *Eur. Phys. J.* **E 5** (2001) 583.

[58] L.D. Landau, E.M. Lifshitz, and L.P. Pitaevskii, *Electrodynamics of Continuous Media*, 2nd ed., Butterworth-Heinemann, 1984.

[59] E. Jarkova, H. Pleiner, H.-W. Müller, and H.R. Brand, *J. Chem. Phys.* **118** (2003) 2422.

[60] P. Kolodner, H. Williams, and C. Mac, *J. Chem. Phys.* **88** (1988) 6512.

[61] E. Blums, A. Mezulis, M. Maiorov, and G. Kronkalns, *J. Magn. Magn. Mater.* **169** (1997) 220.

[62] E. Blums, S. Odenbach, A. Mezulis, and M. Maiorov, *J. Magn. Magn. Mater.* **201** (1999) 268.

[63] E. Blums, *J. Magn. Magn. Mater.* **149** (1995) 111.

[64] S. Odenbach, *J. Magn. Magn. Mater.* **149** (1995) 116.

[65] A. Recktenwald and M. Lücke, *J. Magn. Magn. Mater.* **188** (1998) 326.

[66] P. Bigazzi, S. Ciliberto, and V. Croquette, *J. Phys.(France)* **51** (1990) 611.

[67] M.I. Shliomis, B. Smorodin, *Book of abstracts ICMF9.* Bremen 2001.

[68] J. Boussinesq, *Théorie Analytique de la Chaleur* (Gauthier-Villars, Paris) **II** (1903) 172.

[69] J.K. Platten and G. Chavepeyer, *Int. J. Heat Mass Transf.* **19** (1976) 27.

[70] H.R. Brand, P.C. Hohenberg, and V. Steinberg, *Phys. Rev.* **A 30** (1984) 2548.

[71] A. Abramowitz and I.A. Stegun, *Handbook of Mathematical Functions*, Dover Publications, New York, 1965.

[72] S. Hollinger, M. Lücke, and H.W. Müller, *Phys. Rev.* **E 57** (1998) 4250.

[73] D.T.J. Hurle, E. Jackeman, and E.R. Pike, *Proc. R. Soc. Lond. A* **296** (1967) 469.

[74] S. Chandrasekhar, *Hydrodynamic and hydromagnetic stability*, Clarendon Press, Oxford, 1961.

[75] N. Li, J.O. Murphy, J.M. Steiner, *Z. Angew. Math. Mech.* **75** (1995) 3.

[76] E.N. Lorenz, *J. Atmos. Sci.* **20** (1963) 130.

[77] S. Odenbach, private communication.

[78] H. Pleiner and H.R. Brand, *Hydrodynamics and Electrodynamics of Liquid Crystals* in [84], p.16.

[79] A. Ryskin, H. Pleiner, and H.-W. Müller, *Eur. Phys. J.* **E 11** (2003) 389.

[80] We use rationalized Gaussian (or Heaviside-Lorentz) units. For a conversion to standard SI units see J.D. Jackson, *Classical Electrodynamics*, 2nd edition, Wiley, 1975.

[81] With the usual heuristic definition $\chi = \partial M/\partial H$ there is $\chi = \chi_0 + \chi_H H_0^2$ and $\bar{\epsilon} = 1 + \chi$.

[82] G.K. Auernhammer and H.R. Brand, *Eur. Phys. J.* **B 16** (2000) 157.

[83] In the simplest case this is a 5-mode model for $A_1 = A_0(2 + k)$ and $A_n = 0$ for $n \geq 2$.

[84] A. Buka and L. Kramer (Editors) *Pattern Formation in Liquid Crystals*, Springer, New York, 1996.

[85] S.H. Chen and N.M. Amer, *Phys. Rev. Lett.* **51** (1983) 2298.

[86] S.V. Burylov and Y.L. Raikher, *Mol. Cryst. Liq. Cryst.* **258** (1995) 107.

[87] H. Pleiner, E. Jarkova, H.-W. Müller, and H.R. Brand, *Magnetohydrodynamics* **37** (2001) 254.

[88] In this chapter ν is the dynamic viscosity, while in chapters 2,3 the kinematic viscosity is denoted by ν, the latter differing by a factor $1/\rho$ from the former one.

[89] L.I. Berg, G. Ahlers, and D. Cannell, *Phys. Rev.* **E 48** (1993) 3236.

[90] D. Forster, T.C. Lubensky, P.C. Martin, J. Swift, and P.S. Pershan, *Phys. Rev. Lett.* **26** (1971) 1016.

[91] P.C. Martin, O. Parodi, and P.S. Pershan, *Phys. Rev.* **A 6** (1972) 2401.

[92] P.G. de Gennes and J. Prost, *The Physics of Liquid Crystals*, Clarendon Press, Oxford, 1993.

[93] G. Küppers and D. Lortz, *J. Fluid Mech.* **35** (1969) 609.

[94] Q. Feng, W. Pesch, and L. Kramer, *Phys. Rev.* **A 45** (1992) 45.

[95] F.G. Busse, *J. Fluid Mech.* **52** (1972) 97.

[96] A. Buka, *Viscous Fingering* in [84], p. 291 , and references therein.

[97] P.G. Saffman and G.I. Taylor, *Proc. Roy. Soc. London* **A 245** (1958) 312.

[98] C. Park and G.M. Homsy, *J. Fluid Mech.* **139** (1984) 291.

[99] L. Paterson, *J. Fluid Mech.* **113** (1981) 513.

Acknowledgment
I would like to thank H. Pleiner and H.-W. Müller for supervising my work, M. Lücke for his efforts as Zweitgutachter, as well as him, B. Huke, H.R. Brand, S. Odenbach, and D. Jung for helpful and interesting discussions, the Deutsche Forschungsgemeinschaft (SPP1104) for financial support, and the Max Planck Institute for Polymer Research, Mainz, for hospitality and excellent working conditions.